Bulletin of Engineering Geology and the Environment (2023) 82:269
https://doi.org/10.1007/s10064-023-03309-x

REVIEW PAPER

Characterization of sand particle morphology: state-of-the-art

KV Anusree[1] · Gali Madhavi Latha[1]

Received: 10 February 2023 / Accepted: 11 June 2023 / Published online: 23 June 2023

Abstract
The morphology of granular materials, such as sands, is of significant importance due to the effect of grain shape on their physical, mechanical, and hydraulic behavior. As technology has progressed from visual identification to modern computer-based techniques, numerous methods have been developed for quantifying grain shapes, many of which utilize digital image analysis and advances in computational techniques. A comprehensive understanding of available shape characterization methods is essential to make better use of these tools. This paper presents a state-of-the-art review of current methods for characterizing the morphology of granular materials, focusing particularly on digital image analysis techniques. It critically evaluates two essential aspects of shape characterization: the acquisition of particle shape information and shape measurement methods, discussing the strengths and limitations of each approach. Further, the application of grain shape characterization to analyze the effect of particle shape on the macro-scale behavior of sand is discussed. The review emphasizes the need to shift from classical shape characterizations developed by sedimentologists to objective-oriented shape characterizations that enable micro-to-macro correlations, taking into account the availability of robust tools and technologies.

Keyword Particle shape measurement · Shape descriptors · Digital image analysis · X-ray micro-CT · Spherical harmonics · Fractal methods

Introduction

The mechanical behavior of granular materials is influenced by the underlying micro-mechanisms, which are affected by the particle shape, fabric, contact characteristics, etc. The effect of particle morphology on the physical, mechanical, and hydraulic behavior of aggregates has been widely documented. In the geotechnical engineering context, the shape of sand particles has been found to affect the shear response, packing, stiffness, compressibility, and critical state parameters (Santamarina and Cho 2004; Cho et al. 2006; Cavarretta et al. 2010; Altuhafi et al. 2016). Considering other aspects of construction engineering, the shapes of fine and coarse aggregates significantly influence the strength and properties of concrete mixtures, the performance of asphalt mixes, and the mechanical properties of unbound pavement layers (Barksdale and Itani 1989; Meininger 1998; Masad et al. 2001; Garboczi 2002; Rao et al. 2002; Lee et al. 2019). The importance of considering the grain shape, especially in granular media like sand, is depicted in Fig. 1. As we can see, the grains and pore spaces determine the densification characteristics of sand in unsaturated and saturated conditions, which is one of many macroscopic characteristics influenced by the particle morphology.

Despite the consensus that particle morphology plays an important role in the behavior of granular materials, there is no standard approach to quantify particle morphology or use it in design practices. While the recent technological revolutions in digital imaging have enabled researchers to capture high-resolution images of particles, advancements in computational tools and algorithms have helped them represent particle morphology through comprehensive shape indices. Precise morphological characterization and classification of granular materials and the development of useful correlations between their quantifiable shape characteristics and mechanical behavior will ensure more judicial use of these materials in engineering applications.

Particle size, unlike particle shape, has been extensively used in design-based applications. However, the current practice of size-based classification is counterintuitive for irregularly shaped particles like sands and aggregates unless

✉ Gali Madhavi Latha
madhavi@iisc.ac.in

KV Anusree
anusreekv@iisc.ac.in

[1] Dept. of Civil Engineering, Indian Institute of Science, Bangalore, India

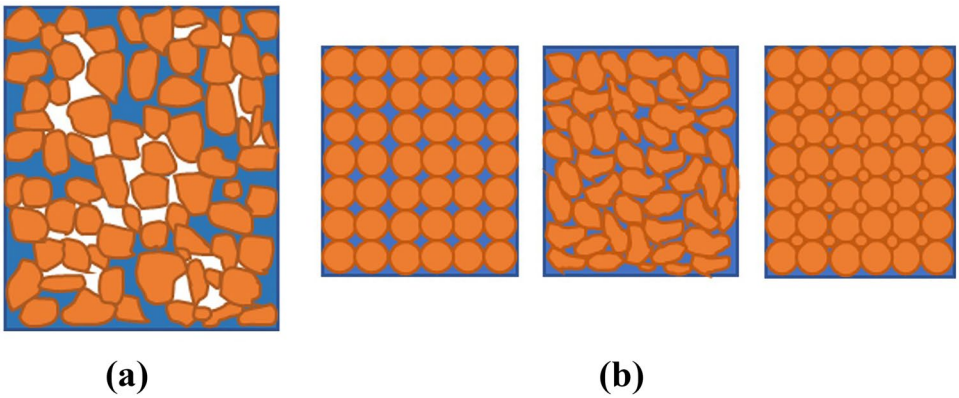

Fig. 1 Schematic diagram showing the effect of morphology of particles on packing: **a** Sand as a granular medium consisting of grains and pore spaces in unsaturated condition; **b** The effect of particle roundness and gradation on particle packing and contacts in a saturated medium

supplemented by shape information. For example, studies reveal that the primary factors affecting the packing of natural sands are particle shape and gradation, not particle size (Youd 1973). Also, the size of an irregularly shaped particle may vary, depending on the method of measurement and the definition of size (Jennings and Parslow 1988). Hence, a more rational and comprehensive choice of morphological parameters of grains and their quantification is necessary for engineering design and practice.

The advent of digital imaging and the development of computers that could store and process large volumes of data are the two factors that contributed to significant advancements in particle shape characterization. Older methods for morphological characterization, like manual measurement and chart-based methods, which were rather cumbersome and subjective, are now being replaced by image analysis methods, which are more accurate, objective, and faster. Advanced techniques such as scanning electron microscopy (SEM) and digital single lens reflex (DSLR) cameras for two-dimensional (2D) analysis and X-ray micro-computed tomography (μCT) and laser scanning for three-dimensional (3D) analysis are being employed to obtain digital images of particles. The high resolution achieved using these instruments has made it possible to characterize particle shapes at unmatched accuracies. Particle characterization in 3D has also facilitated the generation of virtual particles with realistic shape properties to be incorporated into computational models (Liu et al. 2011; Mollon and Zhao 2013, 2014; Zhou and Wang 2017; Su and Yan 2018a). More recently, additive manufacturing of granular particles that exactly mimic the shape characteristics of real ensembles has been successfully demonstrated through computational models developed to recreate the 3D morphology of sand grains (Hanaor et al. 2016; Adamidis et al. 2020; Ahmed and Martinez 2021; Wei et al. 2021).

This article aims to review the state-of-the-art techniques available for the morphological characterization of particles. Emphasis is on methods and descriptors developed based on digital image analysis for geotechnical engineering applications. The article will guide a researcher or practitioner who aims at the morphological characterization of granular materials to select a particular method based on several factors, such as the availability of equipment, complexities involved in the analysis, and the intended purpose.

Description of morphology

The shape of a grain is an expression of its external morphology (Barrett 1980). Describing the shape in a manner that is conceivable by users is as important as obtaining accurate measurements. Several shape descriptors have been developed to qualitatively or quantitively express particle morphology. Qualitative descriptors give a general idea about the shape, using terms such as flaky, elongated, and irregular (Zingg 1935; Krumbein and Pettijohn 1938; Krumbein 1941; Lees 1964; Williams 1965). Researchers have proposed different shape diagrams to classify particle shapes in terms of qualitative descriptors by plotting their dimensional ratios together (Zingg 1935; Sneed and Folk 1958; Blott and Pye 2008). Quantitative shape descriptors can be broadly classified into two categories: geometric shape descriptors and spectral shape descriptors. Geometric shape descriptors represent the grain geometry in ratios or coefficients computed from the geometric measurements on particles, and spectral descriptors represent the grain geometry through harmonic series like the Fourier series and spherical harmonic (SH) series.

The shape of a grain can be expressed at different levels of detail, the features at one level being independent of the other (Wadell 1932, 1933; Wentworth 1933; Krumbein 1941; Pettijohn et al. 1972). Barrett (1980) proposed the expression of shape in terms of three independent properties, viz. form, which describes the overall shape of the particle, roundness which is the mesoscale property describing the overall sharpness of corners; and surface roughness which describes the small-scale features superimposed on roundness (Fig. 2). Attempting a more critical evaluation, the single factors, as proposed by Jia and Garboczi (2016), describe the shape of a particle at different levels of detail, while the

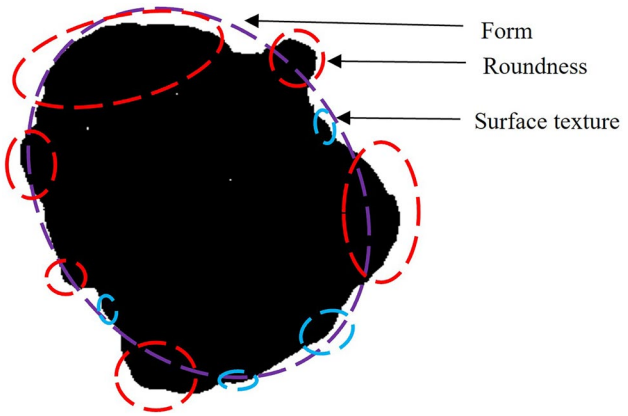

Fig. 2 Different scales of morphology as depicted on a grain projection

parametric series contains information on the entire morphology of the grains, from which the data at any level can be extracted. Parametric series represents a unified approach to characterizing the particle shape. In addition to particle shape description, the expression of particle shape in terms of harmonic series aids the recreation of particle geometry.

The first attempts to quantitatively describe particle shapes have been undertaken by sedimentologists and consisted of manual measurements of particle dimensions, area, volume, etc., to derive shape parameters. Measurements were either performed directly or employed on projected 2D outlines or silhouettes of particles. Since obtaining the 3D shape parameters of grains was challenging, 2D parameters measured on projections of particles were proposed as an alternative. Even though many of these early definitions of shape descriptors haven't been made to define a single level of shape rigidly, these descriptors can be classified into form and roundness/angularity descriptors based on their implications. Particle form is usually measured as the closeness to an ideal shape, and hence form descriptors include the ratios of particle dimensions (which implies the elongation and flatness of the particle) and sphericity (which measures the closeness of the particle shape to a sphere) in 3D and circularity in 2D. While form descriptors thus defined are derived from particle dimensions, area, volume, or the inscribed and circumscribed sphere/circle, the roundness descriptors are used to quantify the sharpness of corners and hence constitute more detailed measurements on the projected particle outline. Wadell (1933) defined roundness as the ratio of average radii of curvature of all corners to the radius of the maximum inscribed circle and suggested that roundness should be distinguished from particle sphericity. Wadell's definition of roundness has prevailed over other definitions due to its functionality. A list of form descriptors derived through direct measurements on the grain or manual measurements on particle silhouettes are provided for 2D and 3D measurements in Tables 1 and 2, respectively. Descriptors that were developed to measure roundness or angularity based on direct 2D measurements on particle projections are given in Table 3.

Morphological characterization using digital image analysis

The evolution of digital image analysis has brought a paradigm shift into particle shape characterizations. Morphological characterization through image analyses involves capturing images of granular materials at sufficient resolutions, applying image processing methods for shape

Table 1 Two-dimensional form descriptors derived through manual measurements on particle silhouettes

Descriptor	Formula	Reference, Remarks
Circularity[a]	$\frac{A}{A_{circle}} = \frac{4\pi A}{P^2}$	Cox (1927) A, P : Area and perimeter of the 2D projection of particle, respectively, A_{circle} : Area of a circle having the same perimeter as the particle projection
Circularity[b]	$\frac{A}{A_{equi}} = \frac{4A}{\pi L^2}$	Pentland (1927) A_{equi} : Area of a circle with a diameter equal to the longest axis of the particle (measured on the particle projection)
Circularity[c] (φ_s)	$\frac{A}{A_c} = \frac{4A}{\pi D_c^2}$	Tickell (1931) A_c : Area of the smallest circumscribing circle, D_c : Diameter of the smallest circumscribing circle
Degree of circularity (C_r)	$\frac{P_{circle}}{P} = \sqrt{\frac{4\pi A}{P^2}}$	Wadell (1933) P_{circle} : Perimeter of a circle having the same area as the particle projection
Degree of sphericity (φ)	$\frac{D_{circle}}{D_c} = \sqrt{\frac{4A}{\pi D_c^2}}$	Wadell (1933) D_{circle} : Diameter of a circle having the same area as the particle projection, D_c : Diameter of the smallest circumscribing circle
Inscribed circle sphericity (φ_o)	$\sqrt{\frac{D_i}{D_c}}$	Riley (1941) D_i : Diameter of the largest inscribed circle, D_c : Diameter of the smallest circumscribing circle

[a,b,c]Authors used the term 'roundness' when in fact, they were measuring sphericity or circularity

Table 2 Three-dimensional form descriptors derived through direct measurements on the particle

Descriptor	Formula	Reference, Remarks
Wentworth flatness index	$\frac{L+I}{2S}$	Wentworth (1922a) L, I, S: Longest, intermediate and shortest axes of the particle
Degree of true sphericity (ψ_s)	$\frac{SA_{sphere}}{SA} = \frac{\sqrt[3]{36\pi V^2}}{SA}$	Wadell (1932) V: Volume of the particle, SA: Surface area of the particle, SA_{sphere}: Surface area of a sphere having the same volume as the particle
Sphericity (ψ_v)	$\sqrt[3]{\frac{V}{V_c}}$	Wadell (1933) V_c: Volume of the smallest circumscribing sphere
Elongation	$\frac{S}{I}$	Zingg (1935)
Flatness	$\frac{I}{L}$	Zingg (1935)
Krumbein intercept sphericity (ψ)	$\sqrt[3]{\frac{IS}{L^2}}$	Krumbein (1941)
Corey Shape Factor	$\frac{S}{\sqrt{LI}}$	Corey (1949)
Aschenbrenner's working sphericity (ψ')	$\frac{12.8\sqrt[3]{p^2q}}{1+p(1+q)+6\sqrt{1+p^2(1+q^2)}}$	Aschenbrenner (1956) $p = \frac{S}{I}, q = \frac{I}{L}$
Aschenbrenner's shape factor (F)	$\frac{LS}{I^2}$	Aschenbrenner (1956)
Maximum projection sphericity (ψ_p)	$\sqrt[3]{\frac{S^2}{LI}}$	Sneed and Folk (1958)
Flatness	$\frac{S}{L}$	Sneed and Folk (1958)
Williams' shape factor (W)	$I - \frac{LS}{I^2}$ *if* $I^2 > LS$, $\frac{I^2}{LS} - 1$ *if* $I^2 \leq LS$	Williams (1965)
Janke's form factor (E)	$\frac{S}{\sqrt{\frac{L^2+I^2+S^2}{3}}}$	Janke (1966)
Oblate-Prolate index	$\frac{10\left(\frac{L-I}{L-S}-0.5\right)}{\frac{S}{L}}$	Dobkins and Folk (1970)

extraction from these images, and quantifying the shape descriptors by analyzing the extracted shape. Further, digital imaging methods are applied to improve the accuracy of measurement of traditional shape descriptors. For example, shape descriptors like roundness and sphericity were historically computed using the equations proposed by Wadell

Table 3 Two-dimensional roundness descriptors derived through manual measurements on particle silhouettes

Descriptor	Formula	Reference, Remarks
Wentworth Shape index	$\frac{D_s}{D_x}$	Wentworth (1919) D_s: Diameter of the circle fitting the sharpest corner, D_x: Diameter of the circle passing through the sharpest corner
Modified Wentworth Shape index	$\frac{D_S}{(L+I)/2}$	Wentworth (1922b) (modified Wentworth (1919) formula) L, I: Length and width of the grain in the projected plane $(L+I)/2$: The mean particle diameter
Roundness	$\frac{\Sigma\left(\frac{r}{R}\right)}{N}$	Wadell (1932) r: Radius of curvature of a corner, R: Radius of maximum inscribed circle, N: Number of corners
Cailleux roundness index	$\frac{D_S}{L}$	Cailleux (1947)
Kuenen roundness index	$\frac{D_S}{I}$	Kuenen (1956)
Angularity (A)	$\sum_{i=1}^{n}\left[(180 - a_i)\frac{x_i}{R}\right]$	Lees (1964) a_i: Angle measured between planes bounding the corner, x_i: Distance from the center of the maximum inscribed circle to the particle tip of the corner
Modified Wentworth roundness	$\frac{D_S}{D_i}$	Dobkins and Folk (1970) D_i: Diameter of the maximum inscribed circle ($D_i = 2R$)
Roundness index	$\frac{D_{s1}+D_{s2}}{D_i}$	Swan (1974) D_{s1}, D_{s2}: Diameters of circles fitting the first two sharpest corners

(1932) through manual measurements of particle dimensions. With the advancements in digital image analysis, computational methods have been proposed to quantify these descriptors automatically, without manual intervention (Zheng and Hryciw 2015; Vangla et al. 2018).

The algorithm proposed by Zheng and Hryciw (2015) is the latest and most widely used technique for the computation of roundness in 2D. The algorithm uses statistical methods of locally weighted regression to remove roughness features, identify corners using key points, and fit circles into the corners by minimizing the distance from the corner points to the circles. Figure 3 shows the circles fit into the corners of grain projections and the maximum inscribed circle for calculation of roundness through digital image analysis. Also, Wadell's definition, which was initially proposed for 2D particle projections, as it was then difficult to measure the 3D geometry of a particle, was later extended to 3D and computational algorithms were proposed for the calculation of 3D roundness (Nie et al. 2018a, b; Zheng et al. 2021). The method for calculation of 2D roundness developed by Zheng and Hryciw (2015) was extended to 3D by Zheng et al. (2021) by developing an algorithm to fit spheres into the corners and ridges. Nie et al. (2018a) proposed an alternate method for 3D roundness calculation in which corner identification was carried out by identifying the vertices with high local curvature and large relative connected areas and then fitting spheres into these corners. Researchers have also developed methods of roundness calculation from the curvature of vertices in the SH reconstructed particle surface (Zhou et al. 2018). More importantly, the measurement of particle roughness or surface texture, which eluded the researchers due to the difficulties in obtaining the images of particles in sufficient resolutions to quantify roughness, has been made possible with advanced imaging methods and image analysis techniques. A summary of form descriptors derived through digital image analysis of 2D and 3D geometries of grains is given in Table 4. Roundness and angularity descriptors developed through image analysis, some of which are also employed in commercial equipment for morphological analysis for 2D and 3D image measurements, are given respectively in Tables 5 and 6. It should be noted that the roughness descriptors derived through image analysis, as shown in Tables 7 and 8, are classified here into 2D and 3D based on whether planar projections or surface profiles at multiple locations or the whole 3D geometry was considered for classification.

However, the method of describing particle shapes using characteristic descriptors suffers many limitations (Zhou et al. 2015). Firstly, a single descriptor is not enough to describe a shape, and selecting the least number of descriptors that can accurately and wholly describe the particle shape becomes imperative. Again, as described above, different researchers propose different descriptors to describe particle morphology, making it difficult to standardize or unify the descriptors in different contexts (Fonseca et al. 2012; Zhou et al. 2015). Using parametric series such as Fourier and SH series was proposed as 'uniform descriptors' to overcome these limitations (Garboczi 2002; Zhou et al. 2015).

Morphological description using parametric series

As mentioned earlier, the shape or outline of a particle can be represented in terms of harmonic series such as the Fourier series or SH functions. It means that the complete details of a particle shape can be described in a limited set of numbers as the coefficients of the terms of the harmonic series. This will considerably reduce the data needed to be stored compared with digital methods, where details of every pixel/voxel of a particle image are to be stored and handled. This is particularly relevant when actual shapes are to be incorporated into computational models. In addition, the representation of shapes in terms of harmonic functions will enable the calculation of different geometric parameters related to the shape

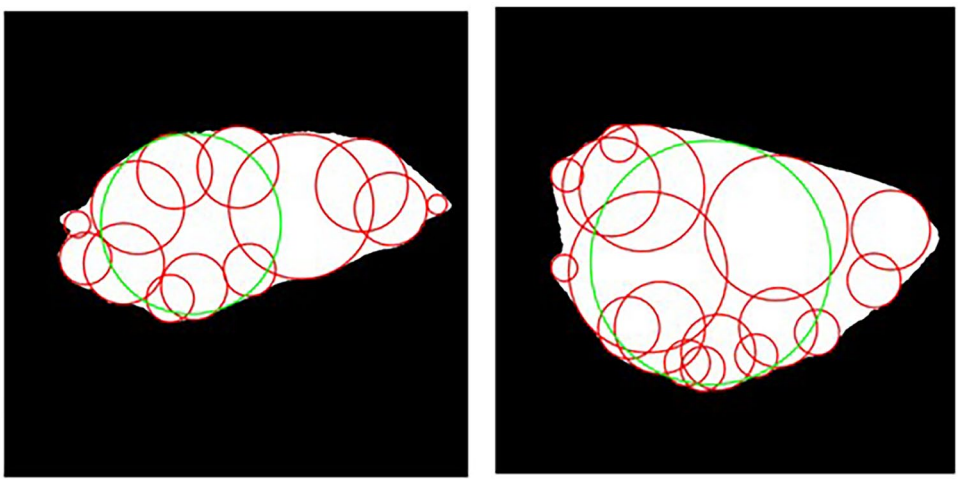

Fig. 3 Corners with best fitting circles (red) and the maximum inscribed circle (green) on binary images of grain projections for the calculation of Wadell's roundness

Table 4 Three-dimensional and two-dimensional form descriptors derived through image analysis operations performed on digital images of particles

Descriptor	Formula	Reference, Remarks
Sphericity (3D)	$\frac{V_p}{V_s}$	Alshibli et al. (2015) V_P: Actual volume of the particle, V_s: Volume of a sphere with diameter equals to the shortest dimension
Inscribed-circumscribed sphere ratio (3D) (ψ_{i-c})	$\frac{D_{i-s}}{D_{c-s}}$	Maroof et al. (2020) D_{i-s}: Diameter of the largest inscribed sphere, D_{c-s}: Diameter of the smallest circumscribing sphere
Form index (2D)	$\sum_{\theta=0}^{\theta=360-\Delta\theta} \frac{\lvert R_{\theta+\Delta\theta} - R_\theta \rvert}{R_\theta}$	Masad et al. (2001) R_θ: Radius of the particle at an angle, θ : the directional angle
Normalized shape factor (2D)	$\frac{\sum_{i=1}^{N} \lvert \alpha_{i\,particle} \rvert}{N \times 45^\circ} \times 100\,(\%)$	Sukumaran and Ashmawy (2001) α_i: Distortion angles, denotes the distortion of the particle outline relative to a circle, N: Number of sampling points
Sphericity index (2D)	$\frac{1}{N}\sum_{i=1}^{N}\left\lvert \frac{D_{equ(i)}}{d_{S(i)}} - \frac{D_{equ(i)}}{d_{L(i)}} \right\rvert$	Alshibli and Alsaleh (2004) D_{equ}: Equivalent particle diameter (diameter of the circle having the same perimeter as the particle), d_L, d_S: Longest and shortest dimension of the projection, N: Number of particles
Area sphericity (2D) (S_A)	$\frac{A_{front}}{A_{top}}$	Arasan et al. (2011a) A_{front}: Area of a particle in front view, A_{top}: Area of a particle in top view
Sphericity (2D)	$\frac{A_a}{A_s}$	Alshibli et al. (2015) A_a: Actual area of the particle, A_s: Area of a circle with diameter equals to the shortest dimension

of the particle, like the surface area, volume, curvatures at a point on the surface, and moment of inertia through relevant mathematical expressions (Garboczi 2002). Another significant advantage of the parametric series representation of particle shape is the feasibility of generating virtual particle shapes, which have representative morphological properties as the original sample, by manipulating the morphological data already available. This finds primary applications in the computational modeling of micro-mechanisms of granular media and the reproduction of realistic shapes through additive manufacturing, as it is challenging and expensive to obtain 3D geometries of a large number of granular materials through available tools like μCT scanning. Also, since the variations in the spatial domain can be related to the variations in the frequency domain, the morphological parameters at different levels of detail, like form, roundness, and surface texture, can be derived from the parametric series, making it a unified method for shape characterization. The detail that can be derived from the parametric series will depend upon the original resolution of the digital image used as the reference. However, the representation of shape descriptors in terms of coefficients of harmonic series is rather abstract when compared to the shape descriptors discussed so far, making it difficult to derive the physical meaning related to the morphology of the particle from the parametric representation, especially for practicing engineers who are not familiar with this nuanced mathematical representation. The concept of Fourier analysis, SH expansion, and fractal methods as unified methods of representing particle shape are discussed.

Fourier analysis method

If a particle can be represented by unique sets of distance (R) vs. angle (θ) as shown in Fig. 4, then the Fourier method in closed form (Ehrlich and Weinberg 1970) can be used to represent particle outline (in 2D) as a Fourier series (Garboczi 2002; Wang et al. 2005; Das 2007; Mollon and Zhao 2012) using Eq. (1):

$$R(\theta) = a_0 + \sum_{n=1}^{N} \left[a_n \cos(n\theta) + b_n \sin(n\theta)\right] \tag{1}$$

where $R(\theta)$ is the radius at an angle θ, N is the total number of harmonics, n is the harmonic number, and a and b are coefficients giving the magnitude and phase for each harmonic.

Shape factor, angularity factor, and surface texture factor can be derived from the Fourier series representation, identifying that the low-frequency terms of the series contribute to the overall shape of the particle, the medium frequency terms contribute to the angularity of the particle, and the high-frequency terms contribute to the surface texture. However, determining the thresholding frequencies by which the shape, angularity, and surface texture are separated could be subjective (Wang et al. 2005). Consequently, authors have suggested different descriptor numbers to correspond to different levels of morphological detail (Wang et al. 2005; Das 2007; Mollon and Zhao 2012).

Table 5 Roundness descriptors derived through image analysis operations performed on 2D digital images of particles

Descriptor	Formula	Reference, Remarks
Angularity index (AI)	$1-\left(\frac{A_{ave}}{A_{max}}\right)$	Wilson and Klotz (1996) A_{ave}: Average of all calculated lengths obtained through Hough transform of the image, A_{max}: Length of the longest line
Roundness index (R_n)	$\frac{4\pi A}{P^2}$	Janoo (1998) A, P : Area and perimeter of the 2D projection of particle, respectively
Angularity index (AI)	$\sum_{\theta=0}^{\theta=360-\Delta\theta}\frac{\lvert R_{P\theta}-R_{EE\theta}\rvert}{R_{EE\theta}}$	Masad et al. (2001) $R_{P\theta}$: Radius of a particle at an angle θ, $R_{EE\theta}$: Radius of the equivalent ellipse at an angle θ
Roundness coefficient (R_c)	$\frac{P^2}{4\pi A}$	Kato et al. (2001)
Angularity Index using outline slope (A_i)	$\sum_{e=0}^{170} e\times P(e)$	Rao et al. (2002) e: Starting angle value for each 10 ° class interval on the particle outline discretized as an n-sided polygon, $P(e)$: Probability that the relative change in slope of the polygon has a value in the range e to $e+10$
Roundness index (I_R)	$\frac{1}{N}\sum_{i=1}^{N}\frac{P_{(i)}}{\pi[0.5\times(d_{S(i)}+d_{L(i)}]}$	Alshibli and Alsaleh (2004) d_L, d_S: Longest and shortest dimension of the projection, N: Number of particles
Angularity index (a) by gradient method	$\sum_{i=1}^{N-3}\lvert\theta_i-\theta_{i+3}\rvert$	Masad et al. (2005) θ: Direction of the gradient vector at each edge point, i: Denotes the i th point on the edge of the particle, N: Total number of points on the edge of the particle
Angularity (K)	$\frac{P}{P_{ellipse}}$	Arasan et al. (2011b) $P_{ellipse}$: Perimeter of the equivalent ellipse
Smoothing angularity index	$\sqrt{\frac{1}{n-1}\sum_{i=1}^{n}(d_i-\bar{d})^2}$	Tafesse et al. (2013) d_i: Distance between two smoothing curves at the i th point along the particle outline, $\bar{d}$: Mean of distance between the two smoothing curves, n: Number of perpendicular segments between the two smoothing curves
Roundness	$\frac{P}{\pi\left(\frac{d_L+d_S}{2}\right)}$	Alshibli et al. (2015) d_L, d_S: Longest and shortest diameters on the particle projection
Angularity index (AI_g) by gradient method	$\sum_{i=0}^{\frac{2\pi}{\Delta\varphi}-1}\left\lvert\theta_{(i+1)\Delta\varphi}-\theta_{i\Delta\varphi}\right\rvert$	Chen et al. (2016) $\theta_{i\Delta\varphi}$: Gradient direction at a directional angle $\varphi=i\Delta\varphi$, $\Delta\varphi$: Incremental angle

The Fourier series expansion, as presented above, is valid only for star-like particles, where the value of R is unique for each θ. For star-like particles, all line segments connecting the center to any point on the particle boundary will lie inside the particle boundary. For non-star-like particles which contain re-entrants or internal bubbles, the value of R is not unique along some directions, as shown in Fig. 5. Even though most naturally occurring granular materials obey this condition (Garboczi 2002), some materials, like carbonate sands, possess concave shell-like structures (Bowman et al. 2001). To tackle this problem, the complex Fourier analysis proposed by Clark (1981) has been adopted (Thomas et al. 1995; Bowman et al. 2001). In complex Fourier analysis, the particle boundary is circumnavigated in the complex plane at a constant speed. A complex function is derived from the complex coordinates of the circumnavigated points (x, y), expressing the coordinates as functions of the Fourier series (Eq. (2)).

$$x_m+iy_m=\sum_{n=-\frac{N}{2}+1}^{+\frac{N}{2}}\left(a_n+ib_n\right)\left[\cos\left(\frac{2\pi nm}{M}\right)+i\sin\left(\frac{2\pi nm}{M}\right)\right] \tag{2}$$

where N is the total number of descriptors, M is the total number of boundary points, m is the index number of the point on the particle, n is the descriptor number, a and b are the descriptor coefficients, and i is the complex square root.

Bowman et al. (2001) identified signature descriptors for different morphological features from the analysis of standard shapes, such that descriptors $n=-1,-2,-3$ give measures of elongation, squareness, and triangularity, and $n=+1$ gives a measure of irregularity.

Even though the Fourier descriptor method does not suffer from the issues faced by re-entrant angles, and there is no need to estimate the centroid of the particle as in the case of the Fourier series method described earlier, the method did not gain much popularity. This was because the total number of points required should be equal to 2^k (where k is a positive integer which dictates the number of descriptors gained from the Fourier analysis), and the points should be spaced equally along the particle boundary. This problem was circumvented by Su and Yan (2018b), who first mapped the points on the particle boundary onto a circle having the same

Table 6 Roundness descriptors derived through image analysis operations performed on 3D digital images of particles

Descriptor	Formula	Reference, Remarks
Angularity factor	$\sum_{p=1}^{N_A}\sum_{q=1}^{N_A}\left[\left(a(p,q)/a_0\right)^2+\left(b(p,q)/a_0\right)^2\right]$	Wang et al. (2012) a, b : Real and imaginary coefficients of the 2D Fast Fourier Transform $Z(p,q)$ of the z coordinates of the aggregate profile $z(x,y)$, a_0: Average height of $z(x,y)$, N_A: Threshold frequency for distinguishing angularity
Roundness (I_R)	$\frac{A_p}{4\pi\left(\frac{d_L+d_I+d_S}{6}\right)^2}$	Alshibli et al. (2015) A_P: Actual 3D surface area of the particle, d_L, d_I, d_S: Longest, intermediate, and shortest diameters of the particle
3D Roundness index (R_i)	$\frac{\sum\left(A_n\frac{k_s}{k_i}\right)}{\sum A_n}$	Zhao and Wang (2016) A_n: Area of the n th triangular element, which is part of the corners on the particle, k_i: Local curvature at this vertex, which could be the maximum principal curvature (k_1), minimum principal curvature (k_2), mean curvature (k_m), or Gaussian curvature (k_G), k_s: The corresponding curvature of the particle's maximum inscribed sphere
Angularity index (AI)	$\frac{\sum_{i=1}^{n}\Delta D_i}{\sum_{i=1}^{n}\Delta\alpha_i}$	Yang et al. (2017) ΔD_i: Angle between the gradient vectors of the i th neighboring couple of the surface points on an aggregate, in degrees, $\Delta\alpha_i$: Angle between the gradient vectors of the i th neighboring couple of the surface points on an ideal sphere, in degrees
3D Roundness (R^{3D})	$\frac{\sum R_c}{n_c R_{insc}}$	Nie et al. (2018a) R_c: Radius of spheres fitted to each corner, n_c: Number of corners (corners have with radius of fitted sphere smaller than R_{insc}), R_{insc}: Radius of the maximum inscribed sphere
Roundness (R)	$\frac{\frac{1}{N}\sum_{i=1}^{N}\frac{1}{k_{1,i}}}{r_{in}}$	Zheng et al. (2020b) N: Number of vertices on corners and ridges, $\frac{1}{k_{1,i}}$: Radius of curvature at the i th vertex on corners and ridges, r_{in}: Radius of maximum inscribed sphere
3D Roundness (R_3)	$\frac{\sum_{i=1}^{n} r_{3,i}}{N r_{3,in}}$	Zheng et al. (2021) $r_{3,i}$: Radius of the i th corner or ridge sphere, N: Number of detected corner and ridge spheres, $r_{3,in}$: Radius of the maximum inscribed sphere

perimeter, such that the distance between neighboring points is preserved while mapping. Then the horizontal and vertical coordinates of the particle boundary can be expressed using the Fourier series as a function of the polar angle φ' associated with each point on the circle (Eqs. (3a) and (3b)).

$$x(\varphi') = a_{x0} + \sum_{n=1}^{N}\left[a_{xn}\cos(n\varphi') + b_{xn}\sin(n\varphi')\right] \tag{3a}$$

$$y(\varphi') = a_{y0} + \sum_{n=1}^{N}\left[a_{yn}\cos(n\varphi') + b_{yn}\sin(n\varphi')\right] \tag{3b}$$

where x and y are coordinates of the particle boundary, N is the total number of harmonics, n is the harmonic number, and a_{x0}, a_{y0}, a_{xn}, a_{yn}, b_{xn}, b_{yn} are the Fourier coefficients.

Su and Yan (2018b) proposed a gradient-based angularity index based on the reconstructed morphology using Eqs. (3a) and (3b). They comment that the method can be used for non-star-like particles also, unlike most approaches for calculating angularity, which can only be used for calculating the angularity of star-like particles (Masad et al. 2005; Chen et al. 2016).

Spherical harmonic expansion

While the Fourier analysis method can describe the geometry of a particle in 2D, SH analysis can be used to describe the 3D particle geometry. The points on the surface of a particle can be described in terms of the distance from the center of mass of the particle to the point R_{ij} and the spherical polar coordinates (θ_i, φ_j). Then the function $r(\theta, \varphi)$ can be described as Eq. (4):

$$r(\theta,\varphi) = \sum_{n=0}^{\infty}\sum_{m=-n}^{n} a_{nm} Y_n^m(\theta,\varphi) \tag{4}$$

where the function $Y_n^m(\theta,\varphi)$ is a spherical harmonic function given by Eq. (5):

$$Y_n^m(\theta,\varphi) = \sqrt{\left(\frac{(2n+1)(n-m)!}{4\pi(n+m)!}\right)} P_n^m(\cos(\theta)) e^{im\varphi} \tag{5}$$

where $P_n^x(x)$ are the associated Legendre functions. Then the SH coefficients a_{nm} can be defined as Eq. (6):

$$a_{nm} = \int_0^{2\pi}\int_0^{\pi} d\varphi d\theta \sin(\theta)\, r(\theta,\varphi) Y_n^{m*} \tag{6}$$

Table 7 Roughness descriptors derived through image analysis operations performed on 2D digital images of particles

Descriptor	Formula	Reference, Remarks
Fullness ratio	$\sqrt{\frac{A}{A_{con}}}$	Kuo et al. (1996) A : Area of the 2D projection of the particle, A_{con} : Area of the convex hull
Fractal dimensions (D_r)	$\frac{2}{m}$	Hyslip and Vallejo (1997) m: Slope coefficient correlating the area and perimeter of the particles in logarithmic scale
Roughness (R_0)	$\frac{P}{\pi \times D_{ave}}$	Kuo et al. (1998) P : Perimeter of the 2D projection of the particle, D_{ave}: Average diameter of the particle
Roughness	$\frac{P}{P_{con}}$	Janoo (1998) P_{con}: Convex perimeter of the particle projection
Convexity (C_x)	$\frac{A}{A_{con}}$	Mora and Kwan (2000) A_{con}: Convex area of the particle projection
Surface parameter[a]	$\frac{A_1 - A_2}{A_1} \times 100$	Masad and Button (2000) A_1, A_2: Areas of objects on an image before and after the erosion-dilation cycles, respectively
Form factor[b]	$\frac{4\pi A}{P^2}$	Masad and Button (2000)
Average roughness (R_a)	$\frac{1}{MN}\sum_{i=1}^{M}\sum_{j=1}^{N}\left\|Z_{ij}\right\|$	Alshibli and Alsaleh (2004) M, N: Numbers of pixels in X and Y directions Z: Surface height at a specific pixel relative to the reference plane ($Z_{ij} = \lambda L_{ij}$), λ: Wavelength used in the scan; and L: Wave value for specific coordinates at the particle surface
Root mean square roughness (R_q)	$\sqrt{\frac{1}{MN}\sum_{i=1}^{M}\sum_{j=1}^{N}Z_{ij}^2}$	Alshibli and Alsaleh (2004)
Skewness (R_{sk})	$\frac{1}{MNR_q^3}\sum_{i=1}^{M}\sum_{j=1}^{N}Z_{ij}^3$	Alshibli and Alsaleh (2004)
Kurtosis (R_{ku})	$\frac{1}{MNR_q^4}\sum_{i=1}^{M}\sum_{j=1}^{N}Z_{ij}^4$	Alshibli and Alsaleh (2004)
Wavelet texture Index (TI_n)	$\frac{1}{3N}\sum_{i=1}^{3}\sum_{j=1}^{N}\left(D_{i,j}(x,y)\right)^2$	Masad et al. (2005) N: Total number of coefficients in a detailed image of the texture, D: Detail coefficient,i: Takes values 1, 2 or 3, for the three detailed images of texture, j: Wavelet coefficient index, (x, y): Location of the coefficients in the transformed domain, n: Decomposition level of the image obtained through wavelet transform
Irregularity index ($I_{(2D)}$)	$\sum \frac{y - x}{y}$	Blott and Pye (2008) x: Distance from the centre of the largest inscribed circle to the nearest point of any concavity, y: distance from the centre of the largest inscribed circle to the convex hull, measured in the same direction as x
Convexity (C)	$\frac{A}{A_{rectangle}}$	Arasan et al. (2011b) $A_{rectangle}$: Area of the bounding rectangle
Regularity (R)	$log\left(\frac{P}{P - P_{con}}\right)$	Mollon and Zhao (2012) P_{con}: Convex perimeter of the particle projection

[a,b]Authors argue that the surface parameter method and form factor are unified methods to characterize particle angularity and roughness, capturing angularity at low resolutions and surface texture at high resolutions

The calculation of volume, surface area, curvature, and moment of inertia can be derived from the SH expansion of the particle geometry. However, the method described here can only be used for star-like particles. For star-like particles, the accuracy of SH expansion can be checked using the value of the Gaussian curvature integrated over the surface (Garboczi 2002). SH expansion also serves as a surface interpolation scheme, such that the surface reconstructed through SH expansion will give a better approximation to the real surface of the particle compared to the digital image, which will always have some digital roughness due to the voxel faces. Thus, using SH expansion can eliminate the overestimation of surface area when counting the voxel faces in a digital image (Garboczi 2002). Even though the SH method as described above, in which the coefficients are computed based on a star-shaped geometry assumption, has found numerous applications (Garboczi 2002, 2011; Masad et al. 2005; Grigoriu

Table 8 Roughness descriptors derived through image analysis operations performed on 3D digital images of particles

Descriptor	Formula	Reference, Remarks
Texture factor (*TF*)	$\sum_{p=1}^{N}\sum_{q=1}^{N}\left[\left(a(p,q)/a_0\right)^2+\left(b(p,q)/a_0\right)^2\right]-AF$	Wang et al. (2012) a, b : Real and imaginary coefficients of the 2D Fast Fourier Transform $Z(p,q)$ of the z coordinates of the aggregate profile $z(x,y)$, a_0: Average height of $z(x,y)$ N: Size of $z(x,y)$ matrix, AF: Angularity factor
Convexity	$\frac{V}{V_{CH}}$	Zhao and Wang (2016) V: Volume of the particle, V_{CH}: Volume of the convex hull enclosing the particle
Surface texture index	$\frac{V_1-V_2}{V_1}\times 100$	Yang et al. (2017) V_1: Volume of the 3D images, in voxel, V_2: Volume of the 3D images after an opening operation, in voxel
3D fractal dimension (D)	$\frac{2}{m}$	Zhou et al. (2018) m: Slope coefficient correlating the total area and total perimeter of the 'islands' or 'lakes' identified through the 'image projection analysis' method in log–log scale
Surface texture using fractal parameters (S_q)	$\left(2\pi\frac{q_c^2C_0}{2D_{PSD}-6}\left(\left(\frac{q_1}{q_c}\right)^{2D_{PSD}-6}-1\right)\right)^{0.5}$	Yang et al. (2019) q: Spatial frequency or wave vector, q_c: Threshold wavevector indicating the length scale separating two morphological scales, D_{PSD}: Fractal dimension relating to the slope of the straight fitting line in the double logarithmic plane of power spectrum density versus q, C_0: Related to the intercept and q_c, q_1: Largest wavevector, relates to the spatial interval (for 3D laser scanner) or the resolution of the interferometer

et al. 2006; Cepuritis et al. 2017a, b; Zhou and Wang 2017; Zhou et al. 2018; Yang et al. 2022), the method will give erroneous results if applied for a general shape particle. The discrepancies due to star-shaped assumption arise because, for a particle with a concave surface, the distance function $r(\theta, \varphi)$ will have multiple values for some (θ, φ), and these values will get 'averaged' during the reconstruction, hence resulting in serious errors in the reconstructed morphology (Su and Yan 2018a).

Garboczi (2011) adopted an error check based on the calculated volume of the particle from the SH coefficients and the volume calculated from the voxel assembly. Any particle whose volume differed by at least 5% from the original voxel-based volume was identified to be non-star shaped particles and discarded from the analysis. The assumption of star-shaped particles resulted in excluding a significant proportion of particles from the sample analyzed. As much as 50%–9%

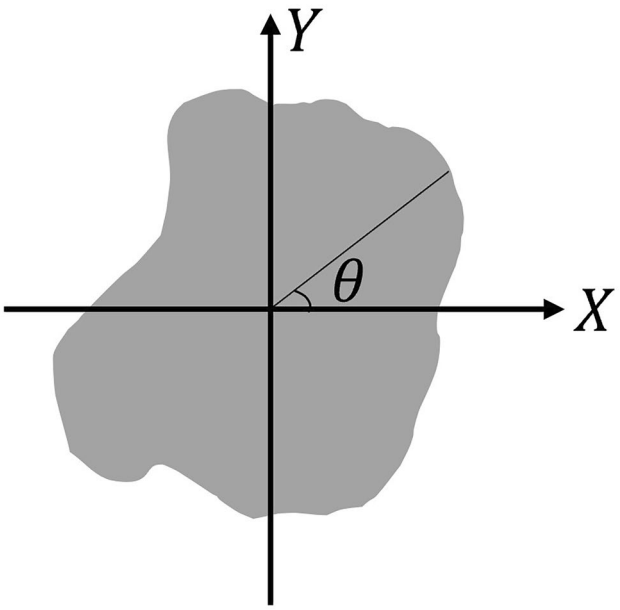

Fig. 4 Fourier analysis representation of particle geometry

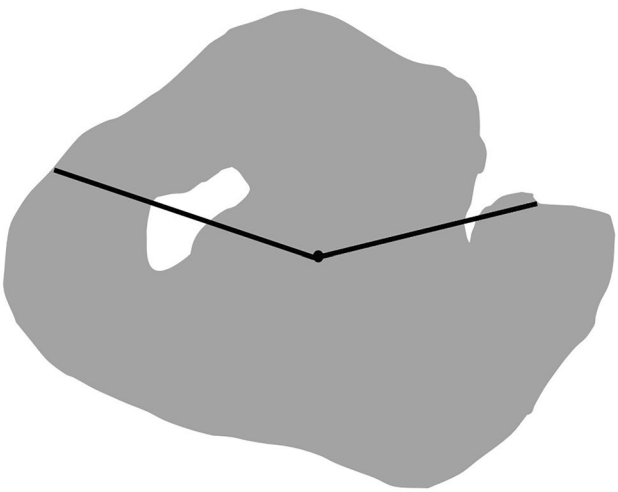

Fig. 5 Difficulties encountered due to re-entrant angles and 'bubbles' in non-star-shaped particles

of particles from different size classes were found to be non-star shaped and hence eliminated. Moreover, Su and Yan (2018a) computed different morphological parameters for a sand sample by considering the star-shaped particle assumption and compared with corresponding values obtained using the SH analysis method for general shape particles. They found that significant differences exist between the parameters calculated from both methods and that by adopting criteria by Garboczi (2011), as much as a quarter of the total number of sand particles in the sample are star-shaped.

The method proposed by Brechbuhler et al. (1995) has been adopted to describe general shaped particles (Zhou et al. 2015; Su and Yan 2018a). In this method, the surface is represented by three simultaneous cartesian coordinate functions, expanded by the SH series (Fig. 6). To follow this method, spherical parametrization is performed in which the surface points are mapped onto a unit sphere. Following spherical parametrization, the coordinates thus obtained are expressed as functions of the corresponding spherical coordinates as Eq. (7).

$$\boldsymbol{X}(\theta,\varphi) = (x(\theta,\varphi), y(\theta,\varphi), z(\theta,\varphi)) \tag{7}$$

then the three coordinates $x(\theta,\varphi), y(\theta,\varphi)$, and $z(\theta,\varphi)$ can be expressed as SH expansions as Eqs. (8a), (8b) and (8c):

$$x(\theta,\varphi) = \sum_{n=0}^{\infty} \sum_{m=-n}^{n} C_{xn}^{m} Y_{n}^{m}(\theta,\varphi) \tag{8a}$$

$$y(\theta,\varphi) = \sum_{n=0}^{\infty} \sum_{m=-n}^{n} C_{yn}^{m} Y_{n}^{m}(\theta,\varphi) \tag{8b}$$

$$z(\theta,\varphi) = \sum_{n=0}^{\infty} \sum_{m=-n}^{n} C_{zn}^{m} Y_{n}^{m}(\theta,\varphi) \tag{8c}$$

where C_{xn}^{m}, C_{yn}^{m}, and C_{zn}^{m} are the SH coefficients for x, y, and z coordinates, respectively, and Y_{n}^{m} is the SH function as defined earlier.

The method was validated for real particles (Zhou et al. 2015; Su and Yan 2018a). Different morphological parameters, such as area, volume, etc., can be derived once the SH expansion of the particle geometry is known. Also, SH degrees associated with different levels of details of morphology have been suggested by different researchers (Masad et al. 2005; Zhou et al. 2015). In addition, the SH reconstructed surface can be further used to compute shape parameters like sphericity or roundness. For example, Zhou et al. (2018) used the SH reconstructed surface to derive roundness based on the principal curvatures of the vertices on the reconstructed particle surface.

In an attempt to reduce the computational effort and the complexities associated with computations, Su and Yan (2018a) proposed that only the real parts of the SH functions can be used to describe the particle geometry (following the method used by Grigoriu et al. (2006) for star shaped particles) and validated the method with the results when the full spectrum was used. However, the degree of expansion of the SH series should be determined based on the accuracy of the details to be reproduced, the original digital resolution of the image, and the computational efforts. Hence, only a truncated SH series expansion is possible, and different researchers have proposed SH degrees in the range of 10–20 for the expansion (Garboczi 2002, 2011; Zhou et al. 2015). One possible drawback associated with the SH method could be the phenomenon of ringing, which arises due to the truncated SH series. Filtering with a Lanczos sigma factor could reduce these ringing artifacts, which will also remove some real surface details but will not affect the overall morphology significantly (Bullard and Garboczi 2013).

SH expansion has been widely used to characterize materials ranging from standard sand particles to rocks to lunar soil simulants (Garboczi and Bullard 2017). Moreover, the SH method has been adopted to generate virtual assemblies of particles with major morphological characteristics of reference sand particles (Grigoriu et al. 2006; Zhou and Wang

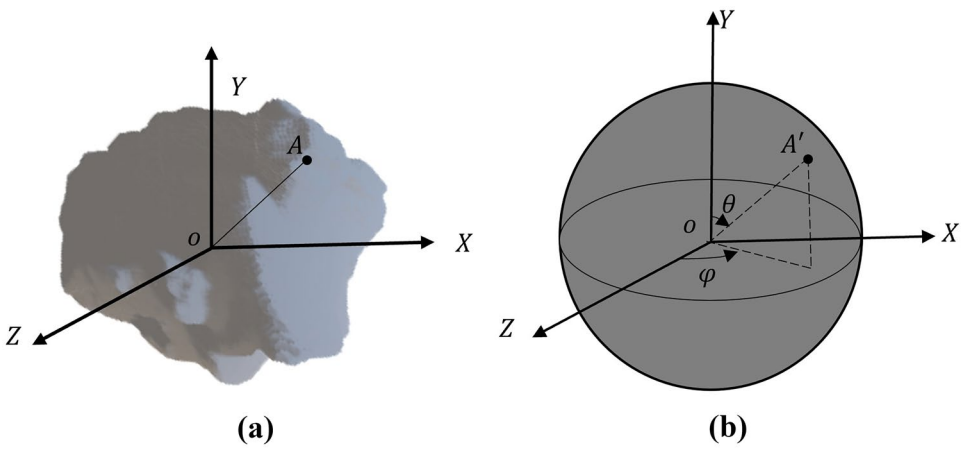

Fig. 6 Illustration of spherical parametrization: **a** Object space; **b** Parameter space

2017; Zhou et al. 2018; Su and Yan 2018a; Sun and Zheng 2021). Grigoriu et al. (2006) used non-Gaussian random field models to generate random star-shaped aggregates virtually. Zhou and Wang (2017) and Zhou et al. (2018) used principal component analysis (PCA) to extract the significant patterns associated with the morphology of natural sand particles from the database constituted by SH coefficients, to generate virtual sand assemblies of two different kinds of sands, which retained major morphological features of the reference sands. Su and Yan (2018a) used PCA and a probabilistic approach to generate 3D virtual sand particles. Wei et al. (2018) used SH descriptors to establish a fractal nature between the multi-scale morphological features and used the relationship to generate artificial grains with major morphological features of original grains. Sun and Zheng (2021) developed a probability-based SH method to create random particles with limited morphological information from a single grain. Alternatively, Mollon and Zhao (2013) and Hanaor et al. (2016) proposed the 3D interpolation of three 2D cross sections to generate random 3D geometries of particles. The 2D surfaces were characterized through Fourier descriptors and fractal geometry. However, the loss of local features due to the artificial selection of the 2D cross sections is an issue in this method (Zhou et al. 2015). These methods help incorporate real particle shapes with different morphological features into computational models to link the micro and macro behavior of sand without having to scan and digitize a large number of sand particles physically. This is especially useful because obtaining the 3D geometry of grains using μCT scanning is expensive, time-consuming, and demands complex and intensive calculations. Tables 9 and 10 give different shape descriptors developed based on the parametric series expansion of particle geometries in 2D and 3D, respectively.

Fractal dimension

Vallejo (1995) introduced the fractal dimensions in the context of the shape description of granular materials. It is argued that the shape of irregular particles formed in nature, like sand grains, is better described by fractal rather than Euclidean geometry (Mandelbrot 1977). The fractal dimension of a rough or fragmented pattern will vary depending on the degree of roughness of the pattern and will have a different value for each pattern type (Kaye 1989). Initially, fractal dimensions have been used to characterize the roughness of the particle (Hyslip and Vallejo 1997; Akbulut 2002; Arasan et al. 2011a). Hyslip and Vallejo (1997) used the parallel line and area-perimeter method to evaluate the fractal dimension of particles, to conclude that the area perimeter method is the easier option. The basic principle behind the divider method, as put forward by Mandelbrot (1983), is that if a line that is irregular at any level of scrutiny is fractal, then the length of the fractal line $P(\lambda)$ can be defined as Eq. (9):

$$P(\lambda) = n\lambda^{1-D_R} \tag{9}$$

where $P(\lambda)$ is the length of the line (curve) based on unit measurement length λ, n is a proportionality constant (equal to the actual and indeterminate length of the line), and D_R

Table 9 Two-dimensional shape descriptors derived based on the parametric series expansion of particle geometries

Descriptor	Formula	Reference, remarks
Signature descriptor coefficient using Fourier descriptor method	$\sqrt{a_n^2 + b_n^2}$	Bowman et al. (2001) a_n, b_n: Fourier descriptor coefficients in the representation of the particle profile, n: Descriptor number $n = -1, -2, -3$ give measures of elongation, triangularity, and squareness, respectively, $n = +1$ gives asymmetry or irregularity, $n = \pm 8$ *to* ± 32 give measure of particle texture
Shape factor, Angularity factor and Surface texture factor using Fourier series (α_i)	$\frac{1}{2}\sum_{n=n_1}^{n_2}\left[\left(\frac{a_n}{a_0}\right)^2 + \left(\frac{b_n}{a_0}\right)^2\right]$	Wang et al. (2005) a_n, b_n: Fourier series coefficients in the representation of the particle profile $n_1 = 1, n_2 = 4$ for Shape factor (α_s) $n_1 = 5, n_2 = 25$ for Angularity factor (α_r) $n_1 = 26, n_2 = 180$ for Surface Texture factor (α_t)
Elongation, and irregularities using Fourier descriptor (D_n)	$\frac{\sqrt{a_n^2 + b_n^2}}{r_0}$	Das (2007) a_n, b_n: Fourier series coefficients in the representation of the particle profile, r_0: Average radius of the particle D_2 describes particle elongation, D_3–D_8 describe main irregularities of the particle contour, D_n for $n > 8$ describes surface irregularities
Gradient based angularity index (AI_g)	$\frac{1}{2\pi}\sum_{i=0}^{w-1}\left\lvert\theta_{(i+1)\Delta\varphi'} - \theta_{i\Delta\varphi'}\right\rvert$	Su and Yan (2018b) φ': Polar angle associated with the boundary point of particle, θ: Gradient direction measuring from the x axis, $\Delta\varphi'$: Step size of the polar angle, $\Delta\varphi' = \frac{2\pi}{w}$, w: Increment factor

Table 10 Three-dimensional shape descriptors derived based on the parametric series expansion of particle geometries

Descriptor	Formula	Reference, remarks
Shape indices using spherical harmonic series (*AI*, *FI*, and *TI*)	$\sum_{n=n_1}^{n_2} \sum_{m=-n}^{n} \lvert a_{nm} \rvert$	Masad et al. (2005) n: Spherical harmonic degree from the 3D particle shape representation as proposed by Garboczi (2002) a_{nm}: Spherical harmonic coefficient at degree n $n_1 = 1, n_2 = 4$ for Form index (*FI*) $n_1 = 5, n_2 = 25$ for Angularity index (*AI*) $n_1 = 26, n_2 = 30$ for Surface Texture index (*TI*)
Volume-surface area shape parameter	$\frac{6V/SA}{VESD}$	Garboczi (2011) V, SA: Volume and surface area of the particle shape, *VESD*: Diameter of a sphere having equal volume as the original particle
Curvature shape parameter	$\frac{2K^{-1}}{VESD}$	Garboczi (2011) K: Mean curvature, integrated over the particle surface area
Angularity index (*AI*)	$\frac{s^2}{2\pi^2} \sum_{\theta=0}^{\pi/s} \sum_{\varphi=0}^{\pi/s} \frac{\lvert r_P - r_{EE} \rvert}{r_{EE}}$	Zhou et al. (2015) s: Step size, r_P: Polar radius with the spherical coordinate (θ, φ), r_{EE}: Polar radius of the equivalent ellipsoid with the spherical coordinate (θ, φ)
3D Roundness (*R*)	$\frac{\sum g(k) \lvert k_{max} \rvert^{-1}}{N R_{ins}}$	Zhou et al. (2018) $g(k) = \begin{cases} 1, \lvert k_{max} \rvert^{-1} < R_{ins} \\ 0, \lvert k_{max} \rvert^{-1} \geq R_{ins} \end{cases}$ $g(k)$ differentiate between corners and non-corners, k_{max}: Maximum principal curvature at a vertex on the SH reconstructed surface, R_{ins}: Radius of the maximum inscribed sphere, N: Total number of corners

is the fractal dimension of the curve which is a quantitative descriptor of roughness.

Thus, if we measure a fractal line various times using increasing measurement length, we will obtain different length values, which, when plotted on a log–log scale, will yield a slope coefficient m, related to the fractal dimension as Eq. (10):

$$D_R = 1 - m \tag{10}$$

The parallel line method, as used by Hyslip and Vallejo (1997), was based on the divider method (Fig. 7). The area-perimeter method is based on the principle that the "ratios of linear extents" of fractal patterns are in themselves fractal (Mandelbrot 1983). The linear extent of a geometrical pattern could mean the length (L), the square root of area ($A^{1/2}$), or the cube-root of volume ($V^{1/3}$). Thus, it can be shown that a linear relationship between area and perimeter on a log–log scale can be derived, with the slope coefficient m related to the fractal dimension D_R as Eq. (11):

$$D_R = {}^{2}/_{m} \tag{11}$$

They also commented that the level of scrutiny with which the grain shape is analyzed would give fractal dimensions corresponding to either the structural or the textural details of the particle shape, relating to structural aspects at a low level of scrutiny and textural aspects at a higher level. The fractal dimension obtained through the area perimeter method was found to correlate with different morphological parameters of various samples, like roundness, convexity, sphericity, and angularity (Vallejo and Zhou 1995; Arasan et al. 2011a). Subsequently, Guida et al. (2020) conducted fractal analysis on the contours of particles and proposed three descriptors to define the shape at the three levels of morphology. More recently, the fractal dimension of aggregate grains has been obtained using the power spectral density function (PSD) of the particle surface (Yang et al. 2016, 2019). The PSD of a surface was calculated as Eq. (12):

$$PSD(q_x, q_y) = \frac{1}{4\pi^2} \iint_{-\infty}^{\infty} A(x,y) e^{-i(xq_x + yq_y)} dxdy \tag{12}$$

where $A(x, y)$ is the auto-correlation function of surface heights $h(x, y)$, and q is the spatial frequency or wavevector.

A threshold value q_c was defined to separate the two morphological scales, i.e., shape and surface texture. The root mean square roughness, S_q (Alshibli and Alsaleh 2004), was then related to the fractal dimensions as Eq. (13):

$$S_q = \left(2\pi \frac{q_c^2 C_0}{2D_{PSD} - 6} \left(\left(\frac{q_1}{q_c} \right)^{2D_{PSD} - 6} - 1 \right) \right)^{0.5} \tag{13}$$

where D_{PSD} is the fractal dimension relating to the slope of the straight fitting line in the double logarithmic plane of power spectrum density versus q, C_0 is related to the intercept, and q_c and q_1 is the largest wavevector, related to the spatial interval (for 3D laser scanner) or the resolution of the interferometer (Yang et al. 2019).

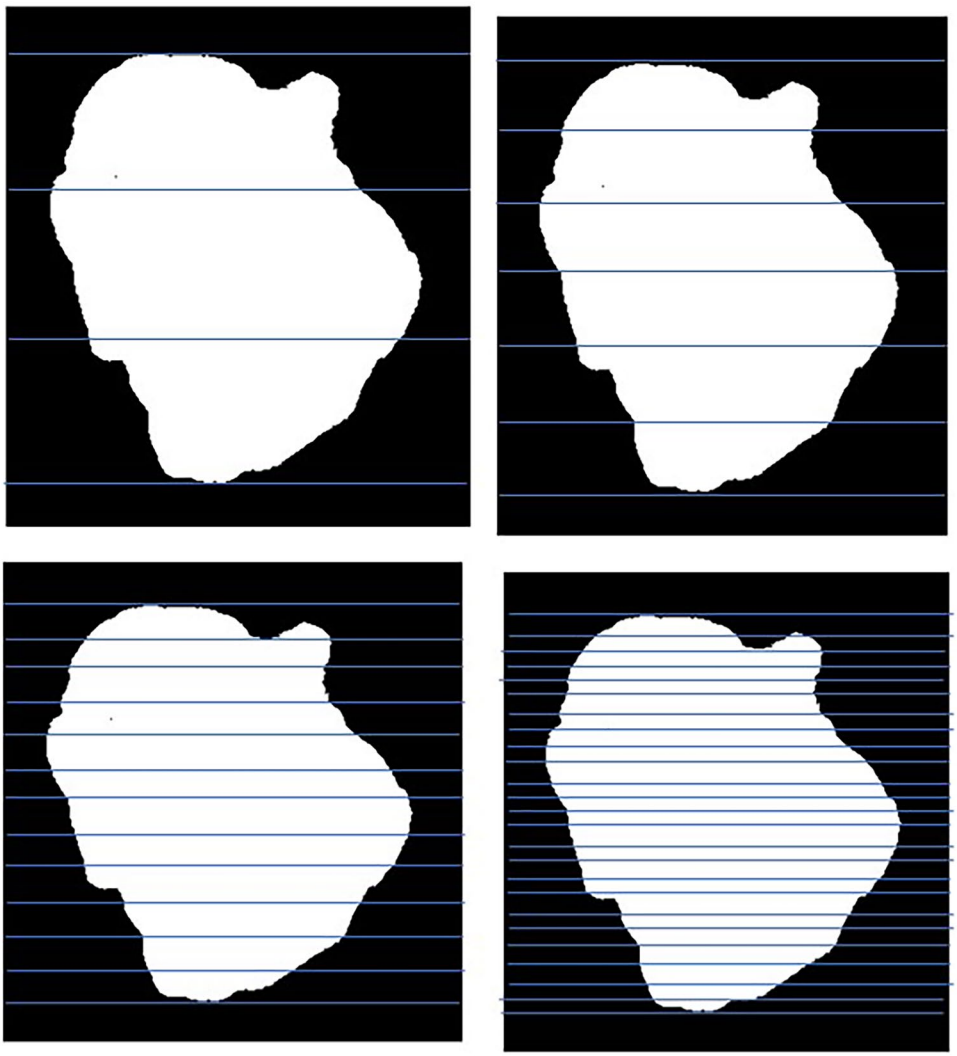

Fig. 7 An example of the parallel line method, the perimeter is measured as the sum polygonal distance between the straight lines; as the step size decreases, the measured polygon perimeter increases

Yang et al. (2022) used this method to bridge the gap between the surface measurements between μCT measurements to characterize shape and interferometer measurements to characterize surface roughness. They identified that some surface details are removed while carrying out an SH expansion with a truncated SH degree. They commented that an SH degree of more than 350 is required to characterize the surface of a particle without losing any details as measured through μCT, which is impractical to adopt during numerical simulations. They also commented that there is a missing scale range in the particle morphology measurement due to the limitations of the current measurement methods. They suggested rebuilding the particle at a multiscale morphology by rebuilding the surface at particle shape scale through SH expansion to a harmonic degree that can be practically achieved and then superimposing the surface texture details by considering the rest of the surface features as the surface texture scale, which can be represented by fractal parameters determined from interferometer measurements. This is a valuable insight that should be considered while incorporating actual particle shapes in computational models. Zhou et al. (2018) applied fractal methods to the entire 3D surface of the particle obtained through μCT measurements. They observed that the triangular prism method proposed by Clarke (1986), or the slit island method proposed by Mandelbrot et al. (1984), which are suitable for 3D open surfaces, are not ideal for 3D closed surfaces such as those of sand particles. They suggested that similar to the slit island method where the fractal surface was 'polished' parallel to the plane base to highlight various closed regions in the open surface, for a closed surface, the particle could be polished spherically to produce a series of closed regions on the spherical polishing surface. The 3D fractal dimension was then derived from the total area and total perimeter of these closed regions.

The methods and descriptors, as discussed above, are not devoid of limitations. Several researchers have attempted the documentation and comparison of these methods based

on their accuracy in describing the desired morphological property, validity of the mathematical procedure, etc. (Mora and Kwan 2000; Masad et al. 2005; Al-Rousan et al. 2007; Tafesse et al. 2013; Sochan et al. 2015; Rorato et al. 2019; Maroof et al. 2020; Su et al. 2020; Zhao et al. 2021).

Shape measurement

The most critical development in morphological characterization results from the automation of shape measurement, brought about by developments in digital imaging and image analysis. The shape measurement methods have evolved from manual measurements of parameters on a single projection photograph or silhouette of a particle to digital processing and analysis of images of thousands of particles at a time using computers. Manual methods, for example, the roundness measurement method adopted by Wadell (1935), are cumbersome, particularly while measuring the shape parameters of a large number of particles. Standard charts were developed to make shape measurement easier, with silhouettes of particles and corresponding measures of sphericity and roundness as reference (Krumbein 1941; Krumbein and Sloss 1951; Powers 1953). However, chart-based methods are highly subjective, depending upon the operator's judgment, and only give information about the 2D morphology of grains. Hryciw et al. (2016) compared the roundness and sphericity values obtained using chart-based methods performed by individuals with those obtained using computer methods for determining particle sphericity and roundness to conclude that the chart-based methods are subjective and inaccurate.

Digital image analysis also replaces direct or indirect measurement methods of particle size and gradation, like calipers, sieving, laser diffraction, etc. (Li and Iskander 2019), giving a more critical and accurate particle size measurement. This is important because the particle size is a parameter that is widely employed for soil classification by many standards and codes (ASTM D6913/6913 M (2017); BS 1377-1 (2016); ISO 11277 (2009)). While standard sieve analysis methods have been developed for particle size determination, it is limited by the lack of precision, ignorance of the particle shape, and practical difficulties while using the apparatus. Also, digital image analysis can standardize the measurements of elongation, flakiness, and angularity, rendering obsolete the current manual, subjective, and inaccurate practices.

2D Measurement methods

2D shape measurement is performed on photographs or projections of grains obtained by using equipment like a digital camera, microscope, or from thin sections depending upon the size of the particle and desired resolution (Kwan et al. 1999; Bowman et al. 2001; Sukumaran and Ashmawy 2001; Fletcher et al. 2003; Fernlund 2005; Altuhafi et al. 2013; Sochan et al. 2015; Vangla et al. 2018; Zhao et al. 2021). Obtained images are pre-processed before carrying out image analysis using computer algorithms to calculate the shape parameters. However, while adopting image-based methods for particle characterization, it's essential to ensure that the images have sufficient resolution such that the computed shape parameters are not affected by the quality of the image being analyzed. Sun et al. (2019a) established the minimum resolution required for accurately estimating morphological parameters at different levels in terms of the particle length, perimeter, and area as controlling factors. At the same time, as image resolution increases, the field of view decreases while using the same equipment, thus making the imaging process more time-consuming and expensive. Hence, a judicial balance between the desired resolution and field of view must be brought about in the scans. It should be noted that 2D imaging systems like SEM can achieve a very high resolution compared to 3D imaging systems (Cepuritis et al. 2017b).

While image-based methods are faster, more accurate, and more robust when compared to manual methods, challenges remain to image a sufficiently large number of particles representative of the soil/specimen being analyzed. The two hurdles researchers encounter while dealing with a large sample are the extraction of individual particle geometries from images of particle assemblies and ensuring a minimum resolution to the image. With the developments in image-based methods, several specialized imaging techniques such as Aggregate Imaging System (AIMS) (Fletcher et al. 2003), Sedimaging (Ohm and Hryciw 2014), Translucent Segregation Table (TST) (Ohm and Hryciw 2013), etc. were developed to obtain the images of a large number of particles at once, without sacrificing the quality of images. However, except where the sample was prepared such that particles were separated from one another before imaging (Kuo et al. 1996; Fernlund 2005; Tafesse et al. 2008; Arasan et al. 2011b; Fletcher et al. 2003), it was necessary to adopt robust segmentation algorithms to automatically segregate the particles digitally before carrying out image analysis. The watershed segmentation method, which can identify the particles, contacts, and voids through their shapes, was first adopted in geotechnical engineering by Ghalib and Hryciw (1999). Though this is a versatile method that can be used for most regularly shaped particles, it is associated with issues like over-segmentation and under-segmentation in the case of highly irregular particles, resulting in erroneous identification of particles and contacts. Hence, a modified watershed method was developed by Zheng and Hryciw (2016a) to resolve these issues in segmentation. By introducing a threshold value for the degree of overlap between

neighboring particles, this new algorithm could accurately distinguish the contacts and particles and helped in the precise segmentation of all particle topologies. Also, for the analysis of a large number of particles and the segregation of particles while imaging, Dynamic Image Analysis (DIA), which was first introduced in the pharmaceutical industry for grain size distribution (Yu and Hancock 2008), was adopted to analyze the morphology of sand grains (Altuhafi et al. 2013; Altuhafi and Coop 2011; Li and Iskander 2019; Sun et al. 2019b; Machairas et al. 2020; Li et al. 2021). An example of a dynamic image analysis system is the QICPIC imaging system (Sympatec 2008), which uses a high frame rate camera with a laser to obtain images of dispersed particles falling through a fall shaft (Altuhafi et al. 2013). The dispersing system prevents the overlapping of particles and allows the imaging of particles at random orientations, as opposed to the preferred orientation of maximum area projections in static imaging systems. The high-speed camera facilitates the capture of hundreds of thousands of images in a short time, thus resulting in statistically relevant shape information from a relatively small sample size. In addition, different camera lenses can be used to scan particle sizes ranging from 7 µm to 3938 µm (Li and Iskander 2019). The device has an inbuilt algorithm that measures several size descriptors and 2D shape descriptors, including convexity, sphericity, and aspect ratio for each particle. However, it should be noted that the device does not directly give the value of Wadell's roundness, which is an important shape parameter. Even then, the images obtained through DIA can be imported and analyzed with any common image analysis software like MATLAB (The Mathworks Inc 2022) or ImageJ (Schneider et al. 2012). Li and Iskander (2019) carried out shape characterization of granular systems with particle size and shape varying over a large range using a QICPIC device (Sympatec 2008) and concluded that DIA could provide accurate shape and size information. However, the smallest particle size that can be scanned should be determined by considering the device's resolution. Altuhafi et al. (2013) suggest that the Feret minimum diameter of the particle (the minimum distance between two tangents on opposite sides of the particle) should be greater than 10 times the pixel size. With current specifications, the minimum particle size is limited to 40 µm for accurate results, while the largest particle size that can be scanned is 4 mm (Li and Iskander 2019). Other limitations associated with the method include the inaccurate imaging of overlapping particles as one particle by the software, in which case special segmentation techniques would have to be adopted to separate the particle images. Also, a commercial particle shape analyzer like QICPIC might not be accessible to everyone.

One of the more challenging tasks of morphological characterization is the extraction of particle shapes from particle assemblies. The methods discussed so far involve sample preparation in the laboratory. However, the characterization of particles in assemblies or with complex backgrounds becomes necessary, especially when the image is taken at a site. In such situations, it is essential to extract the shape of particles that are in full view from these particle assemblies. Zheng and Hryciw (2016b) presented a semi-automated method where full projections of particles are selected manually, followed by which the algorithms developed by Zheng and Hryciw (2015) are employed to compute the roundness and sphericity. The method of manually selecting the full projections is impractical to be used on a large number of particles. Since the problem involved pattern recognition, a method of identifying full projection particles and extracting the boundaries from particle assemblies using machine learning tools was developed by Zheng and Hryciw (2018). They used previously established methods of pattern recognition, such as AdaBoost, to form a strong classifier, divided the training process into stages, and used a sliding window technique to identify full projection particles at different locations. Except for a small number of samples involving complex internal structures and the same color grains, the pattern recognition method performed successfully. Alternatively, Liang et al. (2019) used a lightweight U-net, a deep convolutional neural network, to extract particle shapes from images with complex backgrounds. They also proposed further analysis of the extracted shapes that involved the segmentation of particles using an erosion and flood filling algorithm and the smoothing of extracted particle boundary using a B-spline curve technique. This method also has the advantage of requiring a much lesser number of training images when compared to Zheng and Hryciw (2018). Machine learning techniques also find application in predicting the shape descriptors from input images of either single particles (Kim et al. 2022) or from an assembly of particles (Zheng et al. 2022). Kim et al. (2022) proposed a convolutional neural network (CNN), which is a deep learning technique that can identify and extract discriminative features from images, to compute the shape parameters. The predicted values were compared with mathematically computed values of shape parameters to find that the prediction accuracy depended on the predicted shape parameter. While sphericity, slenderness ratio, and circularity were accurately predicted, the roundness values did not match the directly computed values. They concluded that the errors in the prediction of roundness resulted from the ambiguity of input roundness values in the training data. The ambiguities are attributed to the possibility that the 'ground truth' of roundness value may not be deterministic. Zheng et al. (2022) presented 'Laboratory on a smartphone,' in which they developed a smartphone application based on a machine learning framework that can classify the granular soils based on images of particle assemblies captured using only a smartphone camera, into six roundness classes of very angular,

angular, subangular, subrounded, rounded, and well-rounded soils, according to Powers (1953). The machine learning framework of Zheng et al. (2022) used 60,000 images for the training dataset. They showed that the method could be employed even for challenging images like grains of varying size, the same color, different backgrounds, internal textures, etc., achieving a high accuracy of 93%. The most significant features of the 'Laboratory on a smartphone' technique are that there is no need for specialized equipment to capture the images other than a smartphone camera and no requirement for any computations. This makes the angularity characterization simple and accessible to anyone with a smartphone, allowing real-time evaluations. Such models based on artificial intelligence could overcome the limitations of current image-based methods, such as complicated algorithms, time-intensive calculations, the need for the input of operator-dependent parameters, problems arising from insufficient resolutions of images, etc. (Kim et al. 2022). However, this method cannot provide accurate shape quantifications as of now, apart from classifying the particles into qualitative shape groups. The potential applications of machine learning techniques in morphological characterization seem vast and robust, which are expected to enhance the capabilities of this method in the near future.

Limitations of 2D methods and alternatives

The 2D projection of an irregular particle is not the true representation of its 3D geometry. The 2D image of an irregular particle will depend on the angle at which the image was taken. This is particularly true for sand particles, which are rarely truly spherical. The effect of the angle of projection on the projected surface area of a 3D geometry can be seen in Fig. 8, which shows the 3D rendering of a sand grain and the 2D projections of the same at different angles of projection. From the visual examination, it is clear that the projections exhibit different shapes. Jia and Garboczi (2016) demonstrate this through the example of a cylinder; depending upon the angle at which the image of the cylinder is taken, it could be mistaken for a sphere, disc, rectangular plate, cube, or spherocylinder. However, since 3D imaging systems had only been recently adopted to characterize granular materials, most shape indices are defined on 2D projections, which were relatively easy to acquire. Even today, shape characterization of granular materials is mainly carried out on 2D projections since 3D methods are rather expensive and complex compared to 2D methods, and 3D instruments are not available in most laboratories except where intensive research takes place in the area. 2D and 3D shape indices have been compared for regular geometries like ellipsoids and cylinders and their projections at different projection angles (Vickers 1996; Brown and Vickers 1998; Cavarretta et al. 2009; Yan and Su 2018) or 3D particle geometries obtained through different 3D measurement techniques and their projections or 2D particle images (Kutay et al. 2011; Fonseca et al. 2012; Alshibli et al. 2015; Cepuritis et al. 2017a; Zheng et al. 2019; Su and Yan 2020; Zhao

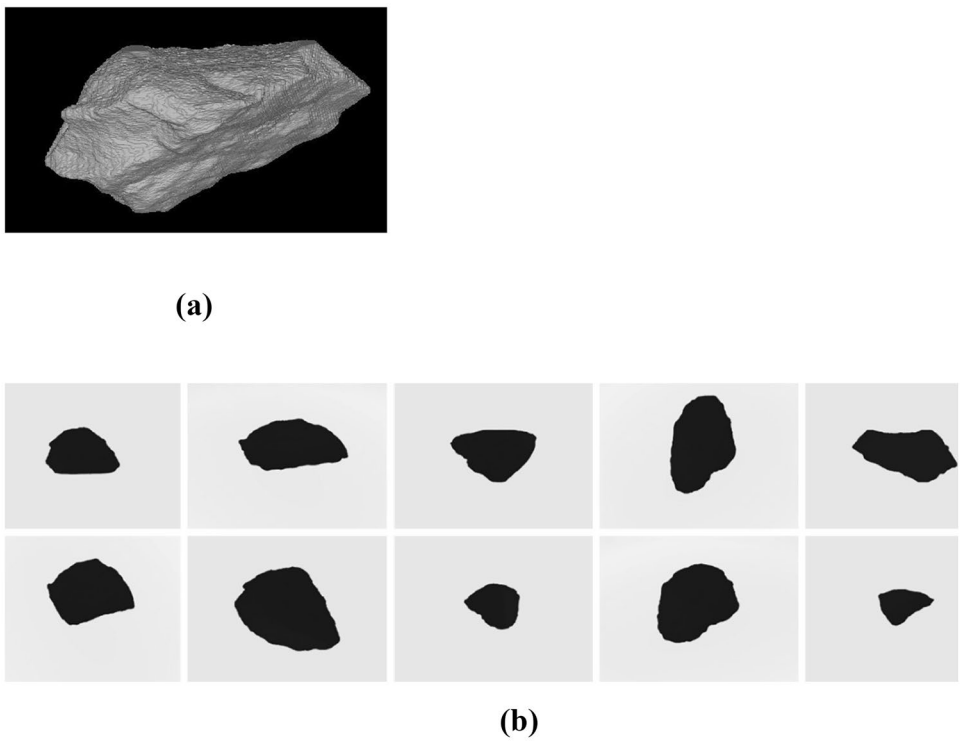

Fig. 8 Effect of the angle of projection on the projected surface area of an image: **a** Three-dimensional image of a particle; **b** Two-dimensional projections of the particle at different projection angles

et al. 2021), and significant differences between obtained 2D and 3D parameters have been reported.

Several techniques have been developed to acquire information about a grain that is not obtainable from its 2D projection. While these methods do not acquire or analyze the entire 3D geometry of the grain, they are developed as simple and cost-effective solutions to collect additional information about the geometry of the grain. When particles are placed on a surface, they tend to lie in the most stable position. Thus, they will have their maximum projection area, and the shortest dimension will be normal to the maximum projection area. The maximum projection area contains information about the longest and intermediate axes of the particle, while the shortest axis cannot be computed. The simplest solution to obtain the third dimension is to obtain more than one image of the particles at directions normal to each other. Researchers have employed various methods, which include a camera setup that is rotated to obtain top and front views of the images (Arasan et al. 2011b), obtaining images of the particles in lying and standing positions (Fernlund 2005; Tafesse et al. 2008, 2012), and attaching particles to transparent trays and obtaining images at two normal orientations (Kuo et al. 1996). All these methods can be said to come under static imaging systems (Tafesse et al. 2012), as they don't have any moving components. Another static imaging system is the Aggregate Imaging System (AIMS), which was developed to image particles at different resolutions, and fields of view using different lighting techniques by scanning particles placed in a glass tray with marked grid points (Fletcher et al. 2003; Mahmoud et al. 2010). Some dynamic imaging systems that were developed include the University of Illinois Aggregate Image Analyzer (UIAIA), which uses three synchronized cameras to image the top, side, and front views of particles as they move on a conveyor belt (Rao and Tutumluer 2000; Rao et al. 2002) and the WipShape system which uses two synchronized cameras to obtain the top and side views of the particles moving on either a conveyor belt or a translucent rotating table (Maerz and Lusher 2001; Maerz 2004). Additionally, a 3D Dynamic Image Analysis (DIA) system has been introduced, which tracks a particle as it falls through the imaging frame and captures the images of the same particle from 8–12 different perspectives, and the size and shape parameters are calculated as average values from these projections (Li and Iskander 2021; Li et al. 2022). The features and performance of 2D and 3D DIA devices have been compared by Li and Iskander (2021) and Li et al. (2022). Sympatec QICPIC and Microtrac PartAn3D were used in these studies for 2D and 3D analysis, respectively. Currently, the image resolutions that can be captured using 2D and 3D DIA devices remain at 4 µm and 15 µm, respectively, and hence the minimum size of the particles that 3D DIA could analyze is higher compared to 2D DIA. In addition to resolution, they differ in terms of the frame rate of the camera, lighting, and algorithm employed. Although 3D DIA is better than 2D DIA, it is inferior to µCT imaging and 3D image analysis.

More advanced methods that can capture the half-particle geometry have been developed to quantify parameters not directly obtained from 2D images. These methods are simpler and cost-effective compared to 3D methods yet acquire more important information compared to 2D methods. Sun et al. (2019c) proposed a structural light system that uses a projector and camera system to analyze the 3D coordinates of particles. It uses the principle that a pattern emitted onto the particle surface will appear differently in the camera view depending upon the surface irregularities. Zheng and Hryciw (2014) used a stereo photography method that uses two parallel images to obtain the 3D contour of particles. The basic concept behind this method was that the information about the third dimension, which is lost when the 3D shape is projected onto a 2D plane, could be recovered by taking a second image offset at a known distance from the first. The imaging setup consisted of a DSLR camera that could be moved vertically and horizontally over a horizontal testing table and controlled through a computer. After the two images have been captured, the techniques of image rectification and point identification are used to obtain the contour map of each particle. After using the methodology to analyze particles of varying sizes, Zheng and Hryciw (2014) observed that the contour lines match the shape and surface topography of the particles well. Kim et al. (2002) developed a laser-based aggregate scanning system to quantify the 3D geometry of particles. The laser scanner uses a laser source and a camera to scan the aggregate sample spread on a horizontal platform. The data points thus acquired are integrated to obtain the half-particle geometry. While these methods can capture the third dimension of particles, which was the intended purpose, they can only capture the half-particle geometry exposed to the camera view. Thus, they fall between 2 and 3D measurements and can be termed '2.5D measurements' (Zheng et al. 2020a). Comparing particle size distribution obtained from 2.5D methods with sieve analysis results showed that these methods can accurately characterize the 3D particle size (Kim et al. 2002; Sun et al. 2019c; Zheng and Hryciw 2014). The application of 2.5D methods to determine 3D shape parameters has been investigated by Zheng et al. (2020a). They compared the shape parameters obtained from 2.5D and 3D geometries of particles and found that while certain shape parameters, including roundness and intercept sphericity, agreed well for the two geometries, convexity did not match the two geometries. It should be noted that 2.5D methods are economical because they require simple equipment, unlike µCT methods. They can overcome the constraints of resolution and

field of view usually associated with μCT devices and scan a higher particle size range, though they cannot match the accuracy of 3D methods.

As discussed earlier, methods of 3D morphological characterization became established only recently, and even then, the methods are often more expensive, complicated, and inaccessible. 2D methods are widely documented and practiced by many researchers. Also, 2D size and shape descriptors are used in design and research to develop correlations with mechanical behavior. Hence, it is logical to try and correlate the 2D shape parameters with its 3D shape properties. Given that a reliable correlation is established, practitioners without access to equipment to capture 3D morphology can utilize these relations to get a more accurate shape characterization using 2D methods. Empirical correlations have been developed to determine the 3D shape parameters from one, two, three, or multiple 2D projections of grains (Kutay et al. 2011; Bagheri et al. 2015; Cepuritis et al. 2017a; Zheng et al. 2020b; Ueda 2022). This research bridges the gap between more accurate, less accessible 3D measurements and the more accessible, less accurate 2D measurements. However, it should be noted that the correlations developed are often limited to a particular type of aggregate in each size range. More importantly, these studies demonstrate that using multiple 2D projections rather than a single image gives more accurate information regarding the morphology of the particle, thus underscoring the limitations of most of the morphological characterization methods that are employed currently.

3D shape measurement methods

The developments in μCT technology in the past two decades, with resolutions achievable in the order of micrometers, can be considered the most significant factor that contributed to the advancements in 3D shape measurement. It is a non-destructive imaging method that can map the surface and interior of a particle through variations in mass density (Stock 2008). During the μCT scanning, the sample is rotated around its axis between an X-ray source and a detector to acquire 2D radiographs. These radiographs are reconstructed using a back projection algorithm to yield the 3D grayscale image of the specimen. In the grayscale image, the grains will have a higher grayscale value, while air or medium surrounding the grains will have a lower grayscale value. The application of μCT scanning in the context of granular geomaterials includes the characterization and visualization of grains (Matsushima et al. 2009; Katagiri et al. 2010, 2015; Garboczi 2011; Fonseca et al. 2012; Alshibli et al. 2015; Zhou et al. 2015, 2018; Cepuritis et al. 2017a, b; Zhao and Wang 2016; Erdogan et al. 2017; Suh et al. 2017; Kong and Fonseca 2018; Su and Yan 2018a; Rorato et al. 2019; Zheng et al. 2019, 2020b; Yang et al. 2022), the evolution of grains and granular fabric under loading (Ando et al. 2013; Druckrey et al. 2016; Druckrey and Alshibli 2016; Alam et al. 2018), and the characterization of the structure of porous media (Al-Raoush and Alshibli 2006). For commercial μCT devices, resolutions usually vary between 1–10 μm, and the maximum specimen size is up to 10 mm (Zhao and Wang 2016). Fonseca et al. (2012), as a rule of thumb, suggested that the voxel size of the image be $0.018 \times d_{50}$, where d_{50} is the median particle diameter. It is to be noted that μCT scanning is a time-intensive process, and the time taken could vary for each instrument, depending on the selected operating conditions. An advancement over the conventional μCT technique is the Synchrotron μCT, which incorporates an X-ray source capable of generating higher intensity beams, resulting in images with higher resolution, less noise, and crisp boundaries (Alshibli et al. 2015; Druckrey and Alshibli 2016). However, the Synchrotron μCT technique is available only with specific research groups. Even though a highly accurate and popular method for 3D imaging, μCT scanning has certain limitations, including the high initial cost, the requirement for a skilled technician for operation and maintenance, and the demand for time and computation. Also, the field of view could be limited due to the constraints in minimum resolution, allowing only the scanning of a small sample size at a time (Garboczi 2002; Zheng et al. 2020b). 3D laser scanning is an alternate method for 3D morphological characterization, which is rather simple and cost-effective compared to μCT scanning (Lanaro and Tolppanen 2002; Hayakawa and Oguchi 2005; Asahina and Taylor 2011; Anochie-Boateng et al. 2013; Sun et al. 2014; Ouhbi et al. 2016). Laser scanning involves emitting light onto the surface of a particle and evaluating the position of each point on the particle based on the time taken by the reflected light or through triangulation. While suitable for granular materials with sizes over a few millimeters, the limited resolution of 3D laser scanning devices often restricts their use for smaller particles (Zhao and Wang 2016). Anochie-Boateng et al. (2013) reported the measurement of particle shape using a laser scanner with the highest resolution of 0.1 mm. The accuracy of the laser scanning technique compared to μCT for measuring the particle geometry of rock fragments with sizes in the range of 2–4 cm was established by Asahina and Taylor (2011). Hayakawa and Oguchi (2005) have reported accurate measurements of the shape of gravel particles using laser scanning. Some other cost-effective options to obtain the 3D geometry of grains include methods based on photogrammetry (Paixao et al. 2018; Zhao et al. 2021) and the reconstruction of the planar projections of the grain acquired at different angles of rotation (Nadimi and Fonseca 2017). The photogrammetry method employed by Paixao et al. (2018) involves imaging a particle rotating on a pedestal from different angles and then employing special algorithms to identify shared features in these images to reconstruct a 3D point cloud. Since the method only requires a digital camera, it costs around one-tenth of a laser scanner. However, the resolution achieved by the setup was around 0.05 mm, which makes it suitable for

only ballast-sized particles. Other possible drawbacks include the requirement of good lighting conditions, the computational effort required to extract the point cloud, and the time taken to scan each particle. Nadimi and Fonseca (2017) used a setup for incremental rotations of the particle so that 2D planar projections could be acquired at different projection angles using a digital camera, which is reconstructed to a 3D volume. The setup only requires a camera and other simple tools and can be easily implemented in a laboratory, making it much more accessible when compared with a μCT scanner. Using this method, it is possible to obtain a resolution of a few micrometers depending on the lens system used, and hence the method is suitable for grains with sizes around 1 mm. However, the method allows scanning only one particle at a time, which is a limitation of the method. It should also be noted that while these methods can obtain information about the particle surface, no information about the internal structure of the particles is obtainable, unlike in μCT scanning.

Image processing is performed on the reconstructed μCT images to obtain the 3D voxel assembly of the particle. Image processing includes the binarization of the grayscale image and image segmentation to extract individual particle geometries before any further image analysis procedure. Before binarization, the noise in raw μCT data is usually removed through filtering. For this purpose, the Gauss and median filters are the most adopted algorithms. Both are filters that operate at a local level; the Gauss filter computes the weighted average over a small local window centered around a voxel to replace the intensity of that voxel with the computed value, whereas the median filter replaces the intensity value of a voxel by the median of the intensity values in its neighborhood. Recently, filters that have a non-local nature, which better preserves the sharpness at the grain-void and grain-to-grain contacts when compared with filters local in nature, have been explored (Vlahinic et al. 2014). Binarization separates the grains from the surrounding medium; in the resulting binary image, the solid voxels corresponding to the particle have a grayscale value of one (appearing white), and the voxels corresponding to the surrounding medium have a grayscale value of zero (appearing black). The most common thresholding technique adopted for binarization is Otsu's thresholding (Otsu 1979), which uses a single intensity threshold to classify voxels into foreground and background. In a binary image, the grains could still be touching each other. To separate and extract the individual grain geometries, segmentation techniques are adopted. The extraction of individual morphologies from an assembly of scanned particles could pose a problem for 3D shape analysis just as it did for the 2D case, especially for μCT devices where the sample is placed in a holding tube and scanned. Some have opted to separate the particles and fix them into a stationary position before imaging by embedding them in a resin or using transparent plastic sheets, or dispersing them in silicone grease or silica oil, such that the contrast in X-ray attenuation rate between the sample and the medium separating the grains will help avoid the need to use complex segmentation algorithms in the later stages (Matsushima et al. 2009; Zhao and Wang 2016; Su and Yan 2018a; Zhou et al. 2018; Yang et al. 2022). However, the sample preparation could be tedious, and in some methods, retrieving the sample from the embedded medium is difficult; hence it is not exactly a non-destructive method.

To segment contacting particles, the watershed segmentation method has been adopted (Faessel and Jeulin 2010; Shi and Yan 2015; Alam and Haque 2017). Watershed analysis detects any constrained areas in the volumetric image and then segments this constrained area, assuming that it corresponds to the contact between two particles. However, this method often fails to give accurate results for highly irregularly shaped particles. Over-segmentation of particles could result in inaccurate size and shape description during the subsequent image analysis (Sun et al. 2019d). The need to eliminate the problem of over-segmentation has prompted different researchers to modify or improve the watershed segmentation technique (Faessel and Jeulin 2010; Shi and Yan 2015; Alam and Haque 2017; Kong and Fonseca 2018; Sun et al. 2019d). Among these methods, those proposed by Kong and Fonseca (2018) and Sun et al. (2019d) gave accurate results for a wide range of particle shapes and sizes without requiring manual intervention. Kong and Fonseca (2018) introduced an adaptive watershed method incorporating an iterative segmentation procedure to refine the segmentation after each iteration. Even though successful in segmenting highly irregularly shaped particles like shelly carbonate sands, the method suffered from complexity and high computational demand. A simpler, faster, improved watershed segmentation technique was developed by Sun et al. (2019d) by extending the improved watershed segmentation technique in 2D developed by Zheng and Hryciw (2016a) into 3D. The method was highly effective in accurately segmenting irregularly shaped particles, successfully eliminating over-segmentation in all the specimens. Alternatively, Vlahinic et al. (2014) developed a level-set-based method to extract the grain geometry directly from the 3D grayscale image in the form of a smooth, continuously differentiable surface. The level set method captures the closed surface through a set of functions called level sets. They argued that the proposed method eliminates the need to convert the grayscale volumetric image into voxels, thus preserving critical information that would otherwise have been lost. This information is important to quantify the physical parameters like the fabric and contact forces. The accuracy of the method was validated by segmenting μCT images of highly irregular and highly rounded geomaterials. Further, Lai and Chen (2019) adopted a machine learning technique called 'trainable Weka Segmentation' and a level-set-based method to segment and reconstruct particles in μCT images

of multi-constituent systems. They observed superior performance of the method over conventional watershed segmentation methods. It is worthwhile to mention that even though there is no commercial equipment for 3D morphological characterization as there exists for 2D shape characterization with built-in particle separation methods and image processing and analysis modules, commercial and open-source software packages are available to perform image processing operations, including segmentation. One popular open-source software worth mentioning is the ImageJ software (Rasband 1997–2011; Abramoff et al. 2004), widely adopted to analyze μCT images (Shi and Yan 2015; Zhou et al. 2018; Yang et al. 2022).

Once the voxel assembly of each particle is obtained through image processing techniques, it can be further used to quantify the particle shape. Mainly, researchers have adopted three approaches to quantify particle shape from the voxel assembly. The first method involves performing direct image analysis and computational operations on voxel assembly to measure the volume, surface area, principal dimensions, and moment of inertia (Lin and Miller 2005; Fonseca et al. 2012; Alshibli et al. 2015; Zhao et al. 2015). However, the scale dependency of the surface area and the saw tooth pattern of the voxelated surface results in discrepancies in the computed surface area (Zhou et al. 2015). The second approach is to reconstruct the particle morphology obtained from the μCT images using different smoothing algorithms and perform computations on the reconstructed surface (Yang et al. 2022). Lin and Miller (2005) and Zhao and Wang (2016) adopted the Marching Cubes algorithm, which assigns probabilities to the voxels and interpolates them based on this information to obtain the reconstructed surface composed of triangular meshes. Alternatively, the surfaces of particles obtained through laser scanning are also divided into triangular sub-surfaces, on which the required calculations are performed (Asahina and Taylor 2011; Anochie-Boateng et al. 2013; Sun et al. 2014). Even though better than the voxel-based approach, the triangulated surface is still not completely continuous and differentiable, resulting in inaccuracies in the computed surface curvatures (Zhou et al. 2018). As discussed previously, the level set-based approach is used to reconstruct the smooth particle surfaces and has superior performance compared to smoothing algorithms like the Marching Cubes algorithm (Vlahinic et al. 2014; Lai and Chen 2019). The third approach is to mathematically characterize the surface of a particle as continuous functions using an SH series, from which the shape parameters can be extracted (Garboczi 2002, 2011; Taylor et al. 2006; Liu et al. 2011; Bullard and Garboczi 2013; Zhou and Wang 2017; Zhou et al. 2018; Su and Yan 2018a; Yang et al. 2022). An earlier section dealt with the representation of 3D particle morphology using the SH expansion. Some of the recent studies are successful in accurately quantifying the particle shape at multiple length scales through spherical harmonic-based fractal analysis (Zhou et al. 2018; Khan and Latha 2023). These studies used μCT scanning of particle assemblies, separation of grain contacts through powerful segmentation algorithms, reconstruction of the 3D grain surfaces using spherical harmonics, and computing 3D shape descriptors from the reconstructed grain surfaces. Figure 9 represents the 3D morphological characterization of a sand particle at different scales using the current, versatile technologies; image acquisition using an μCT device and shape reconstruction and analysis of multi-scale morphology using the SH reconstruction method (Khan and Latha 2023). From Fig. 9, it is evident that 3D characterization gives a more accurate picture of the morphology of grain when compared to 2D characterization, as discussed in the previous section. Different image processing and image analysis techniques adopted by recent studies for 3D morphological characterization of sands are provided in Table 11. It can be seen that much emphasis has been given to μCT reconstruction and subsequent image processing and image analysis techniques in recent times.

Surface roughness measurements

The surface texture of grains has been obtained from 2D or 3D binary images captured at high resolution using SEM, High-Definition cameras, or μCT devices (Masad and Button 2000; Altuhafi et al. 2013; Zheng and Hryciw 2015; Vangla et al. 2018; Zhao and Wang 2016; Yang et al. 2017; Zhou et al. 2018). However, converting grayscale images to binary images results in the loss of information, which will particularly affect the measured texture or roughness more than form and angularity/roundness (Masad et al. 2001). Subsequently, grayscale images have been used to compute surface

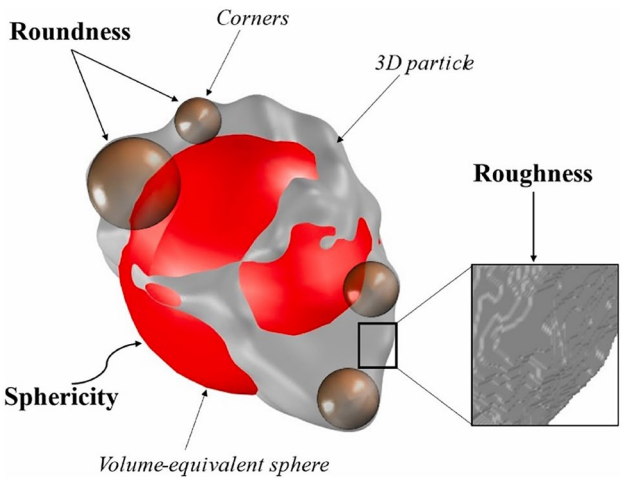

Fig. 9 Three-dimensional morphological characterization of grain at different scales (Khan and Latha 2023)

Table 11 Image processing and image analysis techniques adopted by recent studies for 3D morphological characterization

Study	Image processing technique	Surface smoothing and reconstruction algorithm	Software used
Garboczi (2011)	Thresholding segmentation	Spherical Harmonic (SH) functions	MATLAB, ImagePro
Alshibli et al. (2015)	Filtering based on anisotropic diffusion and interactive segmentation	None	MATLAB, Avizo Fire
Zhao and Wang (2016)	3D Median filtering and thresholding segmentation	Marching Cubes algorithm with a Gaussian filter	MATLAB
Zhou et al. (2018)	3D median filtering, thresholding segmentation and modified 3D watershed segmentation	Spherical Harmonic (SH) functions	MATLAB, ImageJ
Zheng et al. (2020b)	Non-local means filtering and thresholding segmentation	Marching Cubes algorithm	MATLAB, Avizo 9.0
Khan and Latha (2023)	3D median filtering, thresholding segmentation and modified 3D watershed segmentation	Spherical Harmonic (SH) functions	MATLAB

texture (Masad et al. 2001; Fletcher et al. 2003). Currently, to obtain the surface profile of grains, high-resolution optical interferometry is being employed (Alshibli and Alsaleh 2004; Alshibli et al. 2015; Yang et al. 2016, 2019, 2022; Yao et al. 2019). The method yields an interferogram which is a function of sample heights at discrete points. From the interferogram, surface roughness can be computed by quantifying the surface departure from a mean plane (Alshibli et al. 2015) or using the power spectral density function of the surface heights and a fractal method (Yang et al. 2016, 2019, 2022). Generally, since the interferometer measures the surface at a smaller scale, the measurement area is limited; hence, multiple measurements are to be taken at different locations for the same grain (Yao et al. 2019; Yang et al. 2022). To analyze the texture on the entire 3D surface, computations should be done on the surface data obtained by high-resolution μCT measurements (Zhou et al. 2018). However, the analysis will be done on a larger scale, resulting in less accurate measurements. Attempts have been made to correlate the surface texture measured using a large-scale measurement device like a 3D laser scanner or a μCT device and that measured at smaller scales using an interferometer using power spectral density and fractal dimensions so that the measurements made at a larger scale could be extended to a smaller scale for analysis and modeling purposes (Yang et al. 2019, 2022).

A comparison of different equipment used in recent studies to extract 3D morphological information from granular geomaterials, the make of the equipment, and the resolution of image output are given in Table 12. These comparisons show that a variety of equipment is currently available to suit the particle size ranges and resolution requirements. The following section briefly discusses the application of the morphological characterization of grains to correlate the micro and macro-scale behavior of sands. The objective was to understand how developments in morphological characterization could be successfully applied to derive the micro-to-macro correlations rather than to carry out an extensive review of the effect of particle shape characteristics on the macro-scale behavior of sand, as it is out of scope for this paper.

Applications of morphological characterization and the way forward

Following the developments in the morphological characterization of grains, researchers have undertaken several studies to correlate the shape of grains to the physical, mechanical, and hydraulic behavior of sands. The digitization of particle shape measurement enabled fast and accurate characterization of shape for a large number of particles, fueling laboratory experiments using grains with different morphological characteristics (Sukumaran and Ashmawy 2001; Cavarretta et al. 2010; Yang and Luo 2015; Suh et al. 2017; Lakkimsetti and Gali 2023). Further, it provided the basis for incorporating realistic shapes in numerical simulations of granular materials, such as Discrete Element Method (DEM) simulations (Ashmawy et al. 2003; Garcia et al. 2009; Jerves et al. 2016; Nie et al. 2020; Xu et al. 2021). It should be noted that such simulations are particularly helpful in bridging the gap between the continuum and discrete behavior of granular material by facilitating the accurate estimation of micro-mechanisms responsible for macroscopic behavior. In addition, attempts were made to correlate the mechanical properties of sands that have already been documented in the literature to the shape parameters of these sands now obtained through morphological characterization (Altuhafi et al. 2016). The results of these studies demonstrated the dependence of the macroscale properties of sands, such as their fabric, strength, stiffness, and permeability, on the shape of grains. This aspect was also elaborated by Cho

Table 12 Comparison of different equipment adopted by recent studies to extract 3D morphological information from granular geomaterials

Study	Equipment (manufacturer)	Imaging resolution	Size range of particles analyzed
Garboczi (2011)	SkyScan 1172 model (Bruker μCT, USA)	1.3 – 12 μm/voxel	20 μm–300 μm
Fonseca et al. (2012)	Nanotom (PhoenixlX-ray, GE, Germany)	5 μm/voxel	~300 μm
Alshibli et al. (2015)	Beamline 13D, Advanced Photon Source (Argonne National Laboratory, USA)	3.79 μm/voxel	0.297 mm–0.429 mm
Katagiri et al. (2015)	SPring-8 Synchrotron radiation facility (Japan Synchrotron Radiation Research Institute and RIKEN, Japan)	2.0 μm/voxel	105–250 μm
Zhao et al. (2015)	Vltomelx M (GE Phoenix, Germany)	3.3 μm/voxel	1 mm–2 mm
Zhou et al. (2015)	Nanomelx (GE Phoenix, Germany)	10 μm/voxel	1·18 mm–2·36 mm
Zhao and Wang (2016)	Nanomelx (GE Phoenix, Germany)	15 μm/voxel	1 mm–2 mm
Zhou et al. (2018)	Metrotom 1500 (Zeiss, Germany)	32.65 μm/voxel	1·18 mm–2·36 mm
Kong and Fonseca (2018)	Nanotom M (GE Phoenix, Germany)	6.67 μm/voxel	400 μm–2100 μm
Zheng et al. (2020b)	Xradia microXCT-400 (Zeiss, USA)	3 μm/voxel	350 μm–600 μm
Yang et al. (2022)	Toscaner-3000 (Toshiba, Japan)	15.5 μm–18.5 μm/voxel	0.6 mm–2 mm
Li et al. (2022)	PartAn^{3D} (Microtrac, Germany) and QICPIC (Sympatec, Germany)	4–15 μm/pixel	530 μm–2400 μm
Khan and Latha (2023)	SkyScan 1272 model (Bruker μCT, USA)	10 μm/voxel	1 mm–2 mm

et al. (2006), and it was concluded that the current soil classification systems, like the Unified Soil Classification System (USCS), are based on only the size of the particles and overlook the shape. A recommendation was given to provide complete shape characterization of grains along with the size analysis, especially for granular soils.

Particle shape was found to substantially affect the packing of grains, which is one of the important parameters that affect particle-level interactions. Through experimental studies, it was demonstrated that particle regularity affects the maximum and minimum void ratios of an ensemble such that as particles became more irregular, i.e., as their roundness and sphericity decreased, the maximum and minimum void ratios increased (Cho et al. 2006; Altuhafi et al. 2016; Suh et al. 2017). It was postulated that the irregularity hinders the mobility of the particles and thereby reduces their ability to attain denser configurations (Cho et al. 2006). Studies by Santamarina and Cho (2004) and Rodriguez (2013) demonstrated that soil compaction is initiated by particle rotation when equilibrium is disturbed by external forces, and higher sphericity, higher roundness, and lesser roughness contribute to easy rotation and higher compaction. The effect of particle roundness on crushability was investigated by Miura et al. (1997). They found that the crushability increased with the angularity of grains and attributed the increased localized crushing of angular particles at contact points as the reason for this behavior. Particle shape was also found to affect the deformability of sand such that the small strain stiffness decreased with a decrease in the particle roundness and sphericity, whereas an increase in compression and decompression indices was found with decreased regularity of the grains (Cho et al. 2006). Cavarretta et al. (2010) showed that angular particles exhibited greater plasticity during the oedometer tests carried out using crushed glass ballotini as analog soil. They also noted that while the surface roughness of particles influenced the behavior of this soil under compression and shear, angularity and form had a much greater effect on these mechanical properties. A similar observation was made by Altuhafi et al. (2016) that the surface roughness affected the mechanical behavior of sands to a lesser extent compared to other shape parameters. More recent studies by Pillai and Gali (2022, 2023) revealed that particle angularity and roughness could improve the shear response of sand-geosynthetic clay liner interfaces under dry and wet conditions because of increased sand-fiber interlocking and reduced hydration effects.

In addition, experimental and numerical investigations into the effect of particle shape on the liquefaction resistance of sands demonstrated that more angular or irregular particles exhibited greater resistance to liquefaction due to stronger inter-particle contacts and a tighter fabric of irregular particles (Ashmawy et al. 2003; Cho et al. 2006; Yang and Luo 2015; Lakkimsetti and Latha 2022; Lakkimsetti and Gali 2023). Further, particle shape was found to significantly influence the critical state parameters of sand through experimental investigations (Cho et al. 2006; Yang and Luo 2015; Altuhafi et al. 2016; Suh et al. 2017). It was found that, at the critical state, with a decrease in regularity, the critical state friction angle and the intercept of the critical state line increased (Cho et al. 2006). Suh et al. (2017) established relationships between the critical state parameters and the shape parameters and found that the gradient of the critical state line, void ratio intercept, the effective stress ratio at the critical state, and critical state friction angle decreases

with an increase in the overall regularity of the particles. Similar observations were also made from numerical simulations (Jerves et al. 2016; Nie et al. 2020; Xu et al. 2021). An increase in the peak and critical state shear strengths, as well as dilation, was reported with an increase in particle irregularity (Nie et al. 2020; Xu et al. 2021).

The application of 3D printing technology to physically reproduce granular materials with representative shape properties could be viewed as the next big advancement in the field of micro-to-macro correlations of soil properties. For this purpose, 3D printed particles are recreated either from the μCT scans of sand particles or from the artificial digital geometry with desired shape properties created using SH functions. Ahmed and Martinez (2022) carried out bender element tests using 3D printed media with controlled shape parameters and showed that for a given void ratio, relative density, and mean effective stress, higher values of shear wave velocity and shear modulus are achieved for the specimen constituted of particles with higher roundness and sphericity. Similarly, using 3D-printed grains with controlled shapes, Wei et al. (2021) noted a decrease in permeability with an increase in irregular features of the particle surface for uniformly graded specimens with the same porosity.

It should be noted that while most of the experiments with natural sands utilized 2D morphological characterization methods, DEM simulations and experiments using 3D printed media utilized the full 3D information of the grain shape. Going forward, DEM simulations incorporating realistic grain shapes could be the norm in the micro-to-macro linking of granular material characteristics. As 3D-printed granular media can be used for experimental setups that can enable the validation of DEM models, a framework involving 3D morphological characterization, 3D printing of analog particles, and DEM simulations could be expected to bring about breakthrough developments in the understanding of micro-mechanisms responsible for the mechanical behavior of granular materials and hence micro-to-macro correlations.

Conclusions

The paper summarizes various methods developed for characterizing the morphology of granular geomaterials, focusing on the critical review of state-of-the-art techniques. From the analysis of different methods of shape description, imaging, and image processing technique and the application of shape characterization to derive micro-to-macro correlations for sands, the following conclusions are drawn:

- Grain morphology is an important factor that significantly influences the physical and mechanical behavior of sands. Thanks to the advancements in digital imaging and computational capabilities, robust and precise methods for characterizing sand particle morphology are available. These current methods can enable researchers to quantify particle morphology on a routine basis and apply the information thus obtained.
- The number of methods and descriptors available for shape characterization are many, spanning from manual measurement to digital image analysis of 2D and 3D particle geometries. However, while choosing a method of shape characterization, one should be aware of the possibilities and limitations of the method being adopted. State-of-the-art methods provide the most accurate and robust results.
- 3D morphological characterization using μCT technology along with spherical harmonic expansion remains the most versatile method for characterizing grain morphology, with applications that can be extended to the regeneration of virtual grains and computational modeling. However, the higher cost of equipment and the complexity associated with imaging, image processing, and image analysis for 3D methods, when compared with 2D methods, make them less accessible and popular.
- The definitions of particle morphology, such as form, roundness, and roughness, are still mostly those proposed decades earlier by sedimentary geologists, even though the methods of measurements have evolved rather drastically. Since the most critical objective of the morphological characterization of grains is to link the microscopic characteristics to the macroscopic behavior, shape quantifications must be focused on obtaining the most relevant microscopic information.

Declarations

Conflict of interest The authors declare no conflict of interest.

References

Abràmoff MD, Magalhães PJ, Ram SJ (2004) Image Processing with ImageJ Biophotonics Int 11:36–42

Adamidis O, Alber S, Anastasopoulos I (2020) Assessment of three-dimensional printing of granular media for geotechnical applications. Geotech Test J. https://doi.org/10.1520/GTJ20180259

Ahmed SS, Martinez A (2021) Triaxial compression behavior of 3D printed and natural sands. Granul Matter 23:1–21. https://doi.org/10.1007/s10035-021-01143-0

Ahmed SS, Martinez A (2022) Effects of particle shape on the shear wave velocity and shear modulus of 3d printed sand analogs. Open Geomech 3:1–18. https://doi.org/10.5802/ogeo.9

Akbulut S (2002) Fractal dimensioning of sand grains using image analysis system. Pamukkale U J Eng Sci 8:329–334

Alam MF, Haque A (2017) A new cluster analysis-marker-controlled watershed method for separating particles of granular soils. Materials 10:1195. https://doi.org/10.3390/ma10101195

Alam MF, Haque A, Ranjith PG (2018) A study of the particle-level fabric and morphology of granular soils under one-dimensional compression using insitu X-ray CT imaging. Materials 11:919. https://doi.org/10.3390/ma11060919

Al-Raoush R, Alshibli KA (2006) Distribution of local void ratio in porous media systems from 3D X-ray microtomography images. Physica A Stat Mech Appl 361:441–456. https://doi.org/10.1016/j.physa.2005.05.043

Al-Rousan T, Masad E, Tutumluer E, Pan T (2007) Evaluation of image analysis techniques for quantifying aggregate shape characteristics. Constr Build Mater 21:978–990. https://doi.org/10.1016/j.conbuildmat.2006.03.005

Alshibli KA, Alsaleh MI (2004) Characterizing surface roughness and shape of sands using digital microscopy. J Comput Civ Eng 18:36–45. https://doi.org/10.1061/(ASCE)0887-3801(2004)18:1(36)

Alshibli KA, Druckrey AM, Al-Raoush RI, Weiskittel T, Lavrik NV (2015) Quantifying morphology of sands using 3D imaging. J Mater Civ Eng 27:1–10. https://doi.org/10.1061/(ASCE)0887-3801(2004)18:1(36)

Altuhafi FN, Coop MR (2011) Changes to particle characteristics associated with the compression of sands. Géotechnique 61:459–471. https://doi.org/10.1680/geot.9.P.114

Altuhafi F, O'Sullivan C, Cavarretta I (2013) Analysis of an image-based method to quantify the size and shape of sand particles. J Geotech Geoenviron Eng 139:1290–1307. https://doi.org/10.1061/(asce)gt.1943-5606.0000855

Altuhafi FN, Coop MR, Georgiannou VN (2016) Effect of particle shape on the mechanical behavior of natural sands. J Geotech Geoenviron Eng 142:1–15. https://doi.org/10.1061/(ASCE)GT.1943-5606.0001569

Andò E, Viggiani G, Hall SA, Desrues J (2013) Experimental micromechanics of granular media studied by X-ray tomography: recent results and challenges. Géotech Lett 3:142–146. https://doi.org/10.1680/geolett.13.00036

Anochie-Boateng JK, Komba JJ, Mvelase GM (2013) Three-dimensional laser scanning technique to quantify aggregate and ballast shape properties. Constr Build Mater 43:389–398. https://doi.org/10.1016/j.conbuildmat.2013.02.062

Arasan S, Akbulut S, Hasiloglu AS (2011a) The relationship between the fractal dimension and shape properties of particles. KSCE J Civ Eng 15:1219–1225. https://doi.org/10.1007/s12205-011-1310-x

Arasan S, Yenera E, Hattatoglu F, Hinislioglua S, Akbulut S (2011b) Correlation between shape of aggregate and mechanical properties of asphalt concrete: Digital image processing approach. Road Mater Pavement Des 12:239–262. https://doi.org/10.1080/14680629.2011.9695245

Asahina D, Taylor MA (2011) Geometry of irregular particles: Direct surface measurements by 3-D laser scanner. Powder Technol 213:70–78. https://doi.org/10.1016/j.powtec.2011.07.008

Aschenbrenner BC (1956) A new method of expressing particle sphericity. J Sediment Res 26:15–31. https://doi.org/10.1306/74D704A7-2B21-11D7-8648000102C1865D

Ashmawy AK, Hoang VV, Sukumaran B (2003) Evaluating the influence of particle shape on liquefaction behavior using discrete element modeling. The Thirteenth International Offshore and Polar Engineering Conference, Honolulu, Hawai, USA

ASTM D6913/D6913M-17 (2017) Standard test methods for particle-size distribution (gradation) of soils using sieve analysis. ASTM International, West Conshohocken, PA

Bagheri GH, Bonadonna C, Manzella I, Vonlanthen P (2015) On the characterization of size and shape of irregular particles. Powder Technol 270:141–153. https://doi.org/10.1016/j.powtec.2014.10.015

Barksdale RD, Itani SY (1989) Influence of aggregate shape on base behavior. Transp Res Rec 1227:173–182

Barrett PJ (1980) The shape of rock particles, a critical review. Sedimentology 27:291–303. https://doi.org/10.1111/j.1365-3091.1980.tb01179.x

Blott SJ, Pye K (2008) Particle shape: a review and new methods of characterization and classification. Sedimentology 55:31–63. https://doi.org/10.1111/j.1365-3091.2007.00892.x

Bowman ET, Soga K, Drummond W (2001) Particle shape characterisation using Fourier descriptor analysis. Geotechnique 51:545–554. https://doi.org/10.1680/geot.2001.51.6.545

Brechbühler C, Gerig G, Kübler O (1995) Parametrization of closed surfaces for 3-D shape description. Comput vis Image Underst 61:154–170. https://doi.org/10.1006/cviu.1995.1013

British Standards Institute 2016 (2016) Methods of Test for Soils for Civil Engineering Purposes. General Requirements and Sample Preparation. BS 1377-1:2016. London: British Standards Institute

Brown DJ, Vickers GT (1998) The use of projected area distribution functions in particle shape measurement. Powder Technol 98:250–257. https://doi.org/10.1016/S0032-5910(98)00066-7

Bullard JW, Garboczi EJ (2013) Defining shape measures for 3D star-shaped particles: Sphericity, roundness, and dimensions. Powder Technol 249:241–252. https://doi.org/10.1016/j.powtec.2013.08.015

Cailleux A (1947) L'indice d'e´mousse´ des grains de sable et gre`s. Rev Ge´omorph Dyn 3:78–87

Cavarretta I, O'Sullivan C, Coop MR (2009) Applying 2D shape analysis techniques to granular materials with 3D particle geometries. In: Proceedings of 6th International conference on the micromechanics of granular media. Golden, CO, pp 833–836. https://doi.org/10.1063/1.3180057

Cavarretta I, Coop M, O'Sullivan C (2010) The influence of particle characteristics on the behaviour of coarse grained soils. Géotechnique 60:413–423. https://doi.org/10.1680/geot.2010.60.6.413

Cepuritis R, Garboczi EJ, Jacobsen S (2017a) Three dimensional shape analysis of concrete aggregate fines produced by VSI crushing. Powder Technol 308:410–421. https://doi.org/10.1016/j.powtec.2016.12.020

Cepuritis R, Garboczi EJ, Jacobsen S, Snyder KA (2017b) Comparison of 2-D and 3-D shape analysis of concrete aggregate fines from VSI crushing. Powder Technol 309:110–125. https://doi.org/10.1016/j.powtec.2016.12.037

Chen S, Yang X, You Z, Wang M (2016) Innovation of aggregate angularity characterization using gradient approach based upon the traditional and modified Sobel operation. Constr Build Mater 120:442–449. https://doi.org/10.1016/j.conbuildmat.2016.05.120

Cho GC, Dodds J, Santamarina JC (2006) Particle shape effects on packing density, stiffness, and strength: natural and crushed sands. J Geotech Geoenviron Eng 132:591–602. https://doi.org/10.1061/(ASCE)1090-0241(2006)132:5(591)

Clark MW (1981) Quantitative shape analysis: a review. J Int Assoc Math Geol 13:303–320

Clarke KC (1986) Computation of the fractal dimension of topographic surfaces using the triangular prism surface area method. Comput Geosci 12:713–722. https://doi.org/10.1016/0098-3004(86)90047-6

Corey AT (1949) Influence of shape on the fall velocity of sand grains. Dissertation, Colorado A & M College

Cox EP (1927) A method of assigning numerical and percentage values to the degree of roundness of sand grains. J Paleontol 1:179–183

Das N (2007) Modeling three-dimensional shape of sand grains using discrete element method. Dissertation, University of South Florida

Dobkins JE, Folk RL (1970) Shape development on Tahiti-Nui. J Sediment Res 40:1167–1203. https://doi.org/10.1306/74D72162-2B21-11D7-8648000102C1865D

Druckrey AM, Alshibli KA (2016) 3D finite element modeling of sand particle fracture based on in situ X-Ray synchrotron imaging. Int J Numer Anal Methods Geomech 40:105–116. https://doi.org/10.1002/nag.2396

Druckrey AM, Alshibli KA, Al-Raoush RI (2016) 3D characterization of sand particle-to-particle contact and morphology. Comput Geotech 74:26–35. https://doi.org/10.1016/j.compgeo.2015.12.014

Ehrlich R, Weinberg B (1970) An exact method for characterization of grain shape. J Sediment Res 40:205–212. https://doi.org/10.1306/74D71F1E-2B21-11D7-8648000102C1865D

Erdoğan ST, Forster AM, Stutzman PE, Garboczi EJ (2017) Particle-based characterization of Ottawa sand: shape, size, mineralogy, and elastic moduli. Cem Concr Compos 83:36–44. https://doi.org/10.1016/j.cemconcomp.2017.07.003

Faessel M, Jeulin D (2010) Segmentation of 3D microtomographic images of granular materials with the stochastic watershed. J Microsc 239:17–31. https://doi.org/10.1111/j.1365-2818.2009.03349.x

Fernlund JM (2005) Image analysis method for determining 3-D size distribution of coarse aggregates. Bull Eng Geol Environ 64(2):159–166. https://doi.org/10.1007/s10064-004-0251-8

Fletcher T, Chandan C, Masad E, Sivakumar K (2003) Aggregate imaging system for characterizing the shape of fine and coarse aggregates. Transp Res Rec 1832:67–77. https://doi.org/10.3141/1832-09

Fonseca J, O'Sullivan C, Coop MR, Lee PD (2012) Non-invasive characterization of particle morphology of natural sands. Soils Found 52:712–722. https://doi.org/10.1016/j.sandf.2012.07.011

Garboczi EJ (2002) Three-dimensional mathematical analysis of particle shape using X-ray tomography and spherical harmonics: Application to aggregates used in concrete. Cem Concr Res 32:1621–1638. https://doi.org/10.1016/S0008-8846(02)00836-0

Garboczi EJ (2011) Three dimensional shape analysis of JSC-1A simulated lunar regolith particles. Powder Technol 207:96–103. https://doi.org/10.1016/j.powtec.2010.10.014

Garboczi EJ, Bullard JW (2017) 3D analytical mathematical models of random star-shape particles via a combination of X-ray computed microtomography and spherical harmonic analysis. Adv Powder Technol 28:325–339. https://doi.org/10.1016/j.apt.2016.10.014

Garcia X, Akanji LT, Blunt MJ, Matthai SK, Latham JP (2009) Numerical study of the effects of particle shape and polydispersity on permeability. Phys Rev E 80:021304. https://doi.org/10.1103/PhysRevE.80.021304

Ghalib AM, Hryciw RD (1999) Soil particle size distribution by mosaic imaging and watershed analysis. J Comput Civ Eng 13:80–87. https://doi.org/10.1061/(ASCE)0887-3801(1999)13:2(80)

Grigoriu M, Garboczi E, Kafali C (2006) Spherical harmonic-based random fields for aggregates used in concrete. Powder Technol 166(3):123–138. https://doi.org/10.1016/j.powtec.2006.03.026

Guida G, Viggiani GM, Casini F (2020) Multi-scale morphological descriptors from the fractal analysis of particle contour. Acta Geotech 15:1067–1080. https://doi.org/10.1007/s11440-019-00772-3

Hanaor DAH, Gan Y, Revay M, Airey DW, Einav I (2016) 3D printable geomaterials. Géotechnique 66:323–332. https://doi.org/10.1680/jgeot.15.P.034

Hayakawa Y, Oguchi T (2005) Evaluation of gravel sphericity and roundness based on surface-area measurement with a laser scanner. Comput Geosci 31:735–741. https://doi.org/10.1016/j.cageo.2005.01.004

Hryciw RD, Zheng J, Shetler K (2016) Particle roundness and sphericity from images of assemblies by chart estimates and computer methods. J Geotech Geoenviron Eng 142:1–15. https://doi.org/10.1061/(ASCE)GT.1943-5606.0001485

Hyslip JP, Vallejo LE (1997) Fractal analysis of the roughness and size distribution of granular materials. Eng Geol 48:231–244. https://doi.org/10.1016/S0013-7952(97)00046-X

International Organization for Standardization (2009) Soil Quality – Determination of Particle Size Distribution in Mineral Soil Material – Method by Sieving and Sedimentation. ISO 11277:2009. Geneva, Switzerland: International Organization for Standardization

Janke NC (1966) Effect of shape upon the settling velocity of regular convex geometric particles. J Sediment Res 36:370–376. https://doi.org/10.1306/74D714C4-2B21-11D7-8648000102C1865D

Janoo VC (1998) Quantification of shape, angularity, and surface texture of base course materials. US Army Corps of Engineers Cold Regions Research and Engineering Laboratory, Hanover, NH, Special Report 98:1–22

Jennings BR, Parslow K (1988) Particle size measurement: the equivalent spherical diameter. Proc Roy Soc London A Math Phys Sci 419:137–149. https://doi.org/10.1098/rspa.1988.0100

Jerves AX, Kawamoto RY, Andrade JE (2016) Effects of grain morphology on critical state: a computational analysis. Acta Geotech 11:493–503. https://doi.org/10.1007/s11440-015-0422-8

Jia X, Garboczi EJ (2016) Advances in shape measurement in the digital world. Particuology 26:19–31. https://doi.org/10.1016/j.partic.2015.12.005

Katagiri J, Matsushima T, Yamada Y (2010) Statistics on 3D particle shapes of lunar soil (No. 60501) obtained by micro x-ray CT and its image-based DEM simulation. In Earth and Space 2010: Engineering, Science, Construction, and Operations in Challenging Environments, pp 254–259

Katagiri J, Matsushima T, Yamada Y, Tsuchiyama A, Nakano T, Uesugi K, Ohtake M, Saiki K (2015) Investigation of 3D grain shape characteristics of lunar soil retrieved in Apollo 16 using image-based discrete-element modeling. J Aerosp Eng 28:04014092. https://doi.org/10.1061/(ASCE)AS.1943-5525.0000421

Kato Y, Nakata Y, Hyodo M, Murata H (2001) One-dimensional compression properties of crushable soils related to particle characteristics. In: Proceedings of 14th Southeast Asian Geotechnical Conf., Geotechnical Engineering Meeting Society's Meet, Thailand, pp 527–532

Kaye BH (1989) A random walk through fractal dimensions. John Wiley & Sons

Khan R, Latha GM (2023) Multi-scale understanding of sand-geosynthetic interface shear response through Micro-CT and shear band analysis. Geotext Geomembr. https://doi.org/10.1016/j.geotexmem.2023.01.006

Kim H, Haas CT, Rauch AF, Browne C (2002) Dimensional ratios for stone aggregates from three-dimensional laser scans. J Comput Civ Eng 16:175–183. https://doi.org/10.1061/(ASCE)0887-3801(2002)16:3(175)

Kim Y, Ma J, Lim SY, Song JY, Yun TS (2022) Determination of shape parameters of sands: a deep learning approach. Acta Geotech 17:1521–1531. https://doi.org/10.1007/s11440-022-01464-1

Kong D, Fonseca J (2018) Quantification of the morphology of shelly carbonate sands using 3D images. Géotechnique 68:249–261. https://doi.org/10.1680/jgeot.16.P.278

Krumbein WC, Pettijohn FJ (1938) Manual of sedimentary petrography. D Appleton-Century Company Inc, New York

Krumbein WC (1941) Measurement and geological significance of shape and roundness of sedimentary particles. J Sediment Res 11:64–72. https://doi.org/10.1306/D42690F3-2B26-11D7-8648000102C1865D

Krumbein WC, Sloss LL (1951) Stratigraphy and sedimentation. W.H. Freeman and Company, San Francisco

Kuenen PH (1956) Experimental abrasion of pebbles: 2. Rolling by Current J Geol 64:336–368. https://doi.org/10.1086/626370

Kuo CY, Frost JD, Lai JS, Wang LB (1996) Three-dimensional image analysis of aggregate particles from orthogonal projections. Transp Res Rec 1526:98–103. https://doi.org/10.1177/0361198196152600112

Kuo CY, Rollings RS, Lynch LN (1998) Morphological study of coarse aggregates using image analysis. J Mater Civ Eng 10:135–142. https://doi.org/10.1061/(ASCE)0899-1561(1998)10:3(135)

Kutay ME, Ozturk HI, Abbas AR, Hu C (2011) Comparison of 2D and 3D image-based aggregate morphological indices. Int J Pavement Eng 12:421–431. https://doi.org/10.1080/10298436.2011.575137

Kwan AK, Mora CF, Chan HC (1999) Particle shape analysis of coarse aggregate using digital image processing. Cem Concr Res 29:1403–1410. https://doi.org/10.1016/S0008-8846(99)00105-2

Lai Z, Chen Q (2019) Reconstructing granular particles from X-ray computed tomography using the TWS machine learning tool and the level set method. Acta Geotech 14:1–18. https://doi.org/10.1007/s11440-018-0759-x

Lakkimsetti B, Latha GM (2022) Morphological Perspectives to Quantify and Mitigate Liquefaction in Sands. Indian Geotech J 52:1244–1252. https://doi.org/10.1007/s40098-022-00649-5

Lakkimsetti B, Gali ML (2023) Grain Shape Effects on the Liquefaction Response of Geotextile-Reinforced Sands. Int J Geosynth Ground Eng 9:1–17. https://doi.org/10.1007/s40891-023-00434-1

Lanaro F, Tolppanen P (2002) 3D characterization of coarse aggregates. Eng Geol 65:17–30. https://doi.org/10.1016/S0013-7952(01)00133-8

Lee SJ, Lee CH, Shin M, Bhattacharya S, Su YF (2019) Influence of coarse aggregate angularity on the mechanical performance of cement-based materials. Constr Build Mater 204:184–192. https://doi.org/10.1016/j.conbuildmat.2019.01.135

Lees G (1964) A new method for determining the angularity of particles. Sedimentology 3:2–21. https://doi.org/10.1111/j.1365-3091.1964.tb00271.x

Li L, Iskander M (2019) Evaluation of dynamic image analysis for characterizing granular soils. Geotech Test J 43:1149–1173. https://doi.org/10.1520/GTJ20190137

Li L, Iskander M (2021) Comparison of 2D and 3D dynamic image analysis for characterization of natural sands. Eng Geol 290:1–14. https://doi.org/10.1016/j.enggeo.2021.106052

Li L, Beemer RD, Iskander M (2021) Granulometry of two marine calcareous sands. J Geotech Geoenviron Eng 147:1–19. https://doi.org/10.1061/(ASCE)GT.1943-5606.0002431

Li L, Sun Q, Iskander M (2022) Efficacy of 3D dynamic image analysis for characterising the morphology of natural sands. Géotechnique 1–14. https://doi.org/10.1680/jgeot.21.00128

Liang Z, Nie Z, An A, Gong J, Wang X (2019) A particle shape extraction and evaluation method using a deep convolutional neural network and digital image processing. Powder Technol 353:156–170. https://doi.org/10.1016/j.powtec.2019.05.025

Lin CL, Miller JD (2005) 3D characterization and analysis of particle shape using X-ray microtomography (XMT). Powder Technol 154:61–69. https://doi.org/10.1016/j.powtec.2005.04.031

Liu X, Garboczi EJ, Grigoriu M, Lu Y, Erdoğan ST (2011) Spherical harmonic-based random fields based on real particle 3D data: improved numerical algorithm and quantitative comparison to real particles. Powder Technol 207(1–3):78–86. https://doi.org/10.1016/j.powtec.2010.10.012

Machairas N, Li L, Iskander M (2020) Application of dynamic image analysis to sand particle classification using deep learning. In GeoCongress 2020: Modeling, Geomaterials, and Site Characterization, pp 612–621. https://doi.org/10.1061/9780784482803.065

Maerz NH, Lusher M (2001) Measurement of flat and elongation of coarse aggregate using digital image processing. 80th Annual Meeting. Transportation Research Board, Washington DC, pp 2–14

Maerz NH (2004) Technical and computational aspects of the measurement of aggregate shape by digital image analysis. J Comput Civ Eng 18:10–18. https://doi.org/10.1061/(ASCE)0887-3801(2004)18:1(10)

Mahmoud E, Gates L, Masad E, Erdoğan S, Garboczi E (2010) Comprehensive evaluation of AIMS texture, angularity, and dimension measurements. J Mater Civ Eng 22:369–379. https://doi.org/10.1061/(ASCE)MT.1943-5533.0000033

Mandelbrot BB (1977) Fractals: Form, chance and dimension. Freeman, San Francisco

Mandelbrot BB (1983) The fractal geometry of nature. Freeman, San Francisco

Mandelbrot BB, Passoja D, Paullay AJ (1984) Fractal character of fracture surfaces of metals. Nature 308:721–722

Maroof MA, Mahboubi A, Noorzad A, Safi Y (2020) A new approach to particle shape classification of granular materials. Transp Geotech 22:1–13. https://doi.org/10.1016/j.trgeo.2019.100296

Masad E, Button JW (2000) Unified imaging approach for measuring aggregate angularity and texture. Comput Aided Civ Infrastruct Eng 15:273–280. https://doi.org/10.1111/0885-9507.00191

Masad E, Olcott D, White T, Tashman L (2001) Correlation of fine aggregate imaging shape indices with asphalt mixture performance. Transp Res Rec 1757:148–156. https://doi.org/10.3141/1757-17

Masad E, Saadeh S, Al-Rousan T, Garboczi E, Little D (2005) Computations of particle surface characteristics using optical and X-ray CT images. Comput Mater Sci 34:406–424. https://doi.org/10.1016/j.commatsci.2005.01.010

Matsushima T, Katagiri J, Uesugi K, Tsuchiyama A, Nakano T (2009) 3D shape characterization and image-based DEM simulation of the lunar soil simulant FJS-1. J Aerosp Eng 22:15–23. https://doi.org/10.1061/(ASCE)0893-1321(2009)22:1(15)

Meininger RC (1998) Aggregate Tests Related to Performance of Portland Cement Concrete Pavement. National Cooperative Highway Research Program Project 4-20A, Final Report

Miura K, Maeda K, Furukawa M, Toki S (1997) Physical characteristics of sands with different primary properties. Soils Found 37:53–64. https://doi.org/10.3208/sandf.37.3_53

Mollon G, Zhao J (2012) Fourier–Voronoi-based generation of realistic samples for discrete modelling of granular materials. Granul Matter 14:621–638. https://doi.org/10.1007/s10035-012-0356-x

Mollon G, Zhao J (2013) Generating realistic 3D sand particles using Fourier descriptors. Granul Matter 15:95–108. https://doi.org/10.1007/s10035-012-0380-x

Mollon G, Zhao J (2014) 3D generation of realistic granular samples based on random fields theory and Fourier shape descriptors. Comput Methods Appl Mech Eng 279:46–65. https://doi.org/10.1016/j.cma.2014.06.022

Mora CF, Kwan AKH (2000) Sphericity, shape factor, and convexity measurement of coarse aggregate for concrete using digital image processing. Cem Concr Res 30:351–358. https://doi.org/10.1016/S0008-8846(99)00259-8

Nadimi S, Fonseca J (2017) Single-grain virtualization for contact behavior analysis on sand. J Geotech Geoenviron Eng 143:1–10. https://doi.org/10.1061/(ASCE)GT.1943-5606.0001740

Nie Z, Liang Z, Wang X (2018a) A three-dimensional particle roundness evaluation method. Granul Matter 20:1–11. https://doi.org/10.1007/s10035-018-0802-5

Nie Z, Wang X, Liang Z, Gong J (2018b) Quantitative analysis of the three-dimensional roundness of granular particles. Powder Technol 336:584–593. https://doi.org/10.1016/j.powtec.2018.06.020

Nie Z, Fang C, Gong J, Liang Z (2020) DEM study on the effect of roundness on the shear behaviour of granular materials. Comput Geotech 121:103457. https://doi.org/10.1016/j.compgeo.2020.103457

Ohm HS, Hryciw RD (2013) Translucent segregation table test for sand and gravel particle size distribution. Geotech Test J 36:592–605. https://doi.org/10.1520/gtj20120221

Ohm HS, Hryciw RD (2014) Size distribution of coarse-grained soil by sedimaging. J Geotech Geoenviron Eng 140:1–9. https://doi.org/10.1061/(ASCE)GT.1943-5606.0001075

Otsu N (1979) A threshold selection method from gray level histograms. IEEE Trans. Systems, Man, and Cybernetics 9:62–66

Ouhbi N, Voivret C, Perrin G, Roux JN (2016) Railway ballast: grain shape characterization to study its influence on the mechanical behaviour. Procedia Eng 143:1120–1127. https://doi.org/10.1016/j.proeng.2016.06.150

Paixão A, Resende R, Fortunato E (2018) Photogrammetry for digital reconstruction of railway ballast particles–A cost-efficient method. Constr Build Mater 191:963–976. https://doi.org/10.1016/j.conbuildmat.2018.10.048

Pentland A (1927) A method of measuring the angularity of sands. Roy Soc Canada Proc Trans 21(3):43

Pettijohn FJ, Potter PE, Siever R (1972) Sand and Sandstone. Springer-Verlag, Berlin

Pillai AG, Gali ML (2022) Role of particle shape on the shear strength of sand-GCL interfaces under dry and wet conditions. Geotext Geomembr 50(2):262–281. https://doi.org/10.1016/j.geotexmem.2021.11.004

Pillai AG, Gali ML (2023) Engineering benefits of replacing natural sand with manufactured sand in landfill construction. Sci Rep 13:6444. https://doi.org/10.1038/s41598-023-32835-7

Powers MC (1953) A new roundness scale for sedimentary particles. J Sediment Res 23:117–119. https://doi.org/10.1306/D4269567-2B26-11D7-8648000102C1865D

Rao C, Tutumluer E (2000) Determination of volume of aggregates: new image-analysis approach. Transp Res Rec 1721:73–80. https://doi.org/10.3141/1721-09

Rao C, Tutumluer E, Kim IT (2002) Quantification of coarse aggregate angularity based on image analysis. Transp Res Rec 1787:117–124. https://doi.org/10.3141/1787-13

Schneider C, Rasband W., Eliceiri K. (2012)NIH Image to ImageJ: 25 years of image analysis.Nature Forum 9(7): 671–675.

Riley NA (1941) Projection Sphericity J Sediment Res 11:94–95. https://doi.org/10.1306/D426910C-2B26-11D7-8648000102C1865D

Rodriguez JM (2013) Importance of the particle shape on mechanical properties of soil materials. Dissertation, Luleå University of Technology

Rorato R, Arroyo M, Andò E, Gens A (2019) Sphericity measures of sand grains. Eng Geol 254:43–53. https://doi.org/10.1016/j.enggeo.2019.04.006

Santamarina JC, Cho GC (2004) Soil behaviour: The role of particle shape. In: Advances in geotechnical engineering: The Skempton conference, Thomas Telford Publishing, pp 604–617

Shi Y, Yan WM (2015) Segmentation of irregular porous particles of various sizes from X-ray microfocus computer tomography images using a novel adaptive watershed approach. Géotech Lett 5:299–305. https://doi.org/10.1680/jgele.15.00100

Sneed ED, Folk RL (1958) Pebbles in the lower Colorado River, Texas: a study in particle morphogenesis. J Geol 66:114–150. https://doi.org/10.1086/626490

Sochan A, Zieliński P, Bieganowski A (2015) Selection of shape parameters that differentiate sand grains, based on the automatic analysis of two-dimensional images. Sediment Geol 327:14–20. https://doi.org/10.1016/j.sedgeo.2015.07.007

Stock SR (2008) Recent advances in X-ray microtomography applied to materials. Int Mater Rev 53:129–181. https://doi.org/10.1179/174328008X277803

Su D, Yan WM (2018a) 3D characterization of general-shape sand particles using microfocus X-ray computed tomography and spherical harmonic functions, and particle regeneration using multivariate random vector. Powder Technol 323:8–23. https://doi.org/10.1016/j.powtec.2017.09.030

Su D, Yan WM (2018b) Quantification of angularity of general-shape particles by using Fourier series and a gradient-based approach. Constr Build Mater 161:547–554. https://doi.org/10.1016/j.conbuildmat.2017.12.004

Su D, Yan WM (2020) Prediction of 3D size and shape descriptors of irregular granular particles from projected 2D images. Acta Geotech 15:1533–1555. https://doi.org/10.1007/s11440-019-00845-3

Su D, Wang X, Wang X (2020) An in-depth comparative study of three-dimensional angularity indices of general-shape particles based on spherical harmonic reconstruction. Powder Technol 364:1009–1024. https://doi.org/10.1016/j.powtec.2019.10.019

Suh HS, Kim KY, Lee J, Yun TS (2017) Quantification of bulk form and angularity of particle with correlation of shear strength and packing density in sands. Eng Geol 220:256–265. https://doi.org/10.1016/j.enggeo.2017.02.015

Sukumaran B, Ashmawy AK (2001) Quantitative characterisation of the geometry of discrete particles. Geotechnique 51:619–627. https://doi.org/10.1680/geot.2001.51.7.619

Sun Y, Indraratna B, Nimbalkar S (2014) Three-dimensional characterisation of particle size and shape for ballast. Géotech Lett 4:197–202. https://doi.org/10.1680/geolett.14.00036

Sun Q, Zheng J, Li C (2019a) Improved watershed analysis for segmenting contacting particles of coarse granular soils in volumetric images. Powder Technol 356:295–303. https://doi.org/10.1016/j.powtec.2019.08.028

Sun Q, Zheng J, Coop MR, Altuhafi FN (2019b) Minimum image quality for reliable optical characterizations of soil particle shapes. Comput Geotech 114:1–6. https://doi.org/10.1016/j.compgeo.2019.103110

Sun Q, Zheng Y, Li B, Zheng J, Wang Z (2019c) Three-dimensional particle size and shape characterisation using structural light. Géotech Lett 9:72–78. https://doi.org/10.1680/jgele.18.00207

Sun Y, Cai Z, Fu J (2019d) Particle morphomics by high-throughput dynamic image analysis. Sci Rep 9:1–11. https://doi.org/10.1038/s41598-019-46062-6

Sun Q, Zheng J (2021) Realistic soil particle generation based on limited morphological information by probability-based spherical harmonics. Comput Part Mech 8:215–235. https://doi.org/10.1007/s40571-020-00325-6

Swan B (1974) Measures of particle roundness; a note. J Sediment Res 44:572–577. https://doi.org/10.1306/74D72A90-2B21-11D7-8648000102C1865D

Sympatec (2008) Windox - operating instructions release 5.4.1.0, Sympatec, Clausthal-Zellerfeld, Germany

Tafesse S, Fernlund JMR, Bergholm F, Arvidsson M (2008) New method for 3-D size measurements of particles using image analysis. In: The 33rd International Geological Congress, Oslo, Norway

Tafesse S, Fernlund JMR, Bergholm F (2012) Digital sieving-Matlab based 3-D image analysis. Eng Geol 137:74–84. https://doi.org/10.1016/j.enggeo.2012.04.001

Tafesse S, Fernlund JMR, Sun W, Bergholm F (2013) Evaluation of image analysis methods used for quantification of particle angularity. Sedimentology 60:1100–1110. https://doi.org/10.1111/j.1365-3091.2012.01367.x

Taylor MA, Garboczi EJ, Erdogan ST, Fowler DW (2006) Some properties of irregular 3-D particles. Powder Technol 162:1–15. https://doi.org/10.1016/j.powtec.2005.10.013

The MathWorks Inc (2022) MATLAB version: 9.13.0 (R2022). Natick, Massachusetts: The MathWorks Inc. https://www.mathworks.com

Thomas MC, Wiltshire RJ, Williams AT (1995) The use of Fourier descriptors in the classification of particle shape. Sedimentology 42:635–645. https://doi.org/10.1111/j.1365-3091.1995.tb00397.x

Tickell FG (1931) The Examination of Fragmental Rocks. Stanford University Press, Stanford
Ueda T (2022) Estimation of three-dimensional particle size and shape characteristics using a modified 2D–3D conversion method employing spherical harmonic-based principal component analysis. Powder Technol 404:1–13. https://doi.org/10.1016/j.powtec.2022.117461
Vallejo LE (1995) Fractal analysis of granular materials. Geotechnique 45:159–163. https://doi.org/10.1680/geot.1995.45.1.159
Vallejo LE, Zhou Y (1995) The relationship between the fractal dimension and Krumbein's roundness number. Soils Found 35:163–167. https://doi.org/10.3208/sandf1972.35.163
Vangla P, Roy N, Gali ML (2018) Image based shape characterization of granular materials and its effect on kinematics of particle motion. Granul Matter 20:1–19. https://doi.org/10.1007/s10035-017-0776-8
Vickers GT (1996) The projected areas of ellipsoids and cylinders. Powder Technol 86:195–200. https://doi.org/10.1016/0032-5910(95)03049-2
Vlahinić I, Andò E, Viggiani G, Andrade JE (2014) Towards a more accurate characterization of granular media: extracting quantitative descriptors from tomographic images. Granul Matter 16:9–21. https://doi.org/10.1007/s10035-013-0460-6
Wadell H (1932) Volume, shape, and roundness of rock particles. J Geol 40:443–451. https://doi.org/10.1086/623964
Wadell H (1933) Sphericity and roundness of rock particles. J Geol 41:310–331. https://doi.org/10.1086/624040
Wadell H (1935) Volume, shape, and roundness of quartz particles. J Geol 43:250–280. https://doi.org/10.1086/624298
Wang L, Wang X, Mohammad L, Abadie C (2005) Unified method to quantify aggregate shape angularity and texture using Fourier analysis. J Mater Civ Eng 17:498–504. https://doi.org/10.1061/(ASCE)0899-1561(2005)17:5(498)
Wang L, Sun W, Lally EM, Wang A, Druta C, Tutumluer E (2012) Application of LADAR in the Analysis of Aggregate Characteristics. Transportation Research Board of the National Academies, Washington, DC
Wei D, Wang J, Nie J, Zhou B (2018) Generation of realistic sand particles with fractal nature using an improved spherical harmonic analysis. Comput Geotech 104:1–12. https://doi.org/10.1016/j.compgeo.2018.08.002
Wei D, Wang Z, Pereira JM, Gan Y (2021) Permeability of uniformly graded 3D printed granular media. Geophys Res Lett 48:1–12. https://doi.org/10.1029/2020GL090728
Wentworth CK (1919) A laboratory and field study of cobble abrasion. J Geol 27:507–521. https://doi.org/10.1086/622676
Wentworth CK (1922a) A method of measuring and plotting the shapes of pebbles. Bull US Geol Surv 730C:91–114. https://doi.org/10.3133/b730C
Wentworth CK (1922b) The shapes of beach pebbles. US Geol Surv Prof Pap 131C:75–83. https://doi.org/10.3133/pp131C
Wentworth CK (1933) The shapes of rock particles: a discussion. J Geol 41:306–309. https://doi.org/10.1086/624039
Williams EM (1965) A method of indicating pebble shape with one parameter. J Sediment Res 35:993–996. https://doi.org/10.1306/74D713ED-2B21-11D7-8648000102C1865D
Wilson JD, Klotz LD (1996) Quantitative analysis of aggregate based on Hough transform. Transp Res Rec 1530:111–115. https://doi.org/10.1177/0361198196153000114
Xu MQ, Guo N, Yang ZX (2021) Particle shape effects on the shear behaviors of granular assemblies: irregularity and elongation. Granul Matter 23:1–15. https://doi.org/10.1007/s10035-021-01096-4
Yan WM, Su D (2018) Inferring 3D particle size and shape characteristics from projected 2D images: Lessons learned from ellipsoids. Comput Geotech 104:281–287. https://doi.org/10.1016/j.compgeo.2017.11.015
Yang J, Luo XD (2015) Exploring the relationship between critical state and particle shape for granular materials. J Mech Phys Solids 84:196–213. https://doi.org/10.1016/j.jmps.2015.08.001
Yang H, Baudet BA, Yao T (2016) Characterization of the surface roughness of sand particles using an advanced fractal approach. Proc R Soc A 472:20160524. https://doi.org/10.1098/rspa.2016.0524
Yang X, Chen S, You Z (2017) 3D voxel-based approach to quantify aggregate angularity and surface texture. J Mater Civ Eng 29:1–10. https://doi.org/10.1061/(ASCE)MT.1943-5533.0001872
Yang HW, Lourenço SD, Baudet BA, Choi CE, Ng CW (2019) 3D Analysis of gravel surface texture. Powder Technol 346:414–424. https://doi.org/10.1016/j.powtec.2019.01.074
Yang HW, Lourenço SD, Baudet BA (2022) 3D fractal analysis of multi-scale morphology of sand particles with μCT and interferometer. Géotechnique 72:20–33. https://doi.org/10.1680/jgeot.19.P.120
Yao T, Baudet BA, Lourenço SD (2019) Quantification of the surface roughness of quartz sand using optical interferometry. Meccanica 54:741–748. https://doi.org/10.1007/s11012-018-0879-2
Youd TL (1973) Factors controlling maximum and minimum densities of sands. In: Evaluation of Relative Density and Its Role in Geotechnical Projects Involving Cohesionless Soils, pp 98–112
Yu W, Hancock BC (2008) Evaluation of dynamic image analysis for characterizing pharmaceutical excipient particles. Int J Pharm 361:150–157. https://doi.org/10.1016/j.ijpharm.2008.05.025
Zhao B, Wang J, Coop MR, Viggiani G, Jiang M (2015) An investigation of single sand particle fracture using X-ray micro-tomography. Géotechnique 65:625–641. https://doi.org/10.1680/geot.4.P.157
Zhao B, Wang J (2016) 3D quantitative shape analysis on form, roundness, and compactness with μCT. Powder Technol 291:262–275. https://doi.org/10.1016/j.powtec.2015.12.029
Zhao L, Zhang S, Deng M, Wang X (2021) Statistical analysis and comparative study of multi-scale 2D and 3D shape features for unbound granular geomaterials. Transp Geotech 26:1–12. https://doi.org/10.1016/j.trgeo.2020.100377
Zheng J, Hryciw RD (2014) Soil particle size characterization by stereophotography. In: Geotechnical Special Publication, pp 64–73
Zheng J, Hryciw RD (2015) Traditional soil particle sphericity, roundness and surface roughness by computational geometry. Géotechnique 65:494–506. https://doi.org/10.1680/geot.14.P.192
Zheng J, Hryciw RD (2016a) Segmentation of contacting soil particles in images by modified watershed analysis. Comput Geotech 73:142–152. https://doi.org/10.1016/j.compgeo.2015.11.025
Zheng J, Hryciw RD (2016b) Roundness and sphericity of soil particles in assemblies by computational geometry. J Comput Civ Eng 30:1–13. https://doi.org/10.1061/(ASCE)CP.1943-5487.0000578
Zheng J, Hryciw RD (2018) Identification and characterization of particle shapes from images of sand assemblies using pattern recognition. J Comput Civ Eng 32:1–13. https://doi.org/10.1061/(ASCE)CP.1943-5487.0000765
Zheng W, Hu X, Tannant DD, Zhang K, Xu C (2019) Characterization of two-and three-dimensional morphological properties of fragmented sand grains. Eng Geol 263:1–18. https://doi.org/10.1016/j.enggeo.2019.105358
Zheng J, Sun Q, Zheng H, Wei D, Li Z, Gao L (2020a) Three-dimensional particle shape characterizations from half particle geometries. Powder Technol 367:122–132. https://doi.org/10.1016/j.powtec.2020.03.046
Zheng W, Hu X, Tannant DD (2020b) Shape characterization of fragmented sand grains via X-ray computed tomography imaging. Int J Geomech 20:1–14. https://doi.org/10.1061/(ASCE)GM.1943-5622.0001599
Zheng J, He H, Alimohammadi H (2021) Three-dimensional Wadell roundness for particle angularity characterization of granular soils. Acta Geotech 16:133–149. https://doi.org/10.1007/s11440-020-01004-9

Zheng J, Zhang Z, Li C, Li Z, Gao L (2022) Laboratory-on-a-smartphone for estimating angularity of granular soils. Acta Geotech 17:2651–2674. https://doi.org/10.1007/s11440-021-01259-w

Zhou B, Wang J, Zhao B (2015) Micromorphology characterization and reconstruction of sand particles using micro X-ray tomography and spherical harmonics. Eng Geol 184:126–137. https://doi.org/10.1016/j.enggeo.2014.11.009

Zhou B, Wang J (2017) Generation of a realistic 3D sand assembly using X-ray micro-computed tomography and spherical harmonic-based principal component analysis. Int J Numer Analy Methods Geomech 41:93–109. https://doi.org/10.1002/nag.2548

Zhou B, Wang J, Wang H (2018) Three-dimensional sphericity, roundness and fractal dimension of sand particles. Géotechnique 68:18–30. https://doi.org/10.1680/jgeot.16.P.207

Zingg T (1935) Beitrag zur schotteranalyse. Schweiz Mineral Petrogr Mitt 15:39–140